ABSTRACT

YADAV, PRACHI RAJENDRA. Shape Memory Effect on Plasmon Coupling in Shape Memory Polymers with Embedded Gold Nanoparticles. (Under the direction of Dr. Joseph Tracy).

The organization of Au nanoparticles (NPs) dispersed in polymers determines their optical properties with respect to the interparticle distances and extent of plasmon coupling. In this study, plasmon coupling of spherical Au NPs with an average diameter of 16 nm dispersed in a shape memory polymer (SMP) was investigated. These films were deformed by mechanical stretching and shape recovery was driven thermally. Stretched samples exhibit polarization-dependent responses to light. The optical absorbance maximum corresponding to the surface plasmon resonance is redshifted by up to 21 nm and blueshifted by up to 13 nm for polarization parallel and perpendicular to the stretching direction, respectively. This result can be explained by non-uniform stretching on the nanoscale, where clustering is enhanced along the shear direction as Au NPs are pulled into each other during stretching, while coupling perpendicular to the to the stretching direction is reduced despite the Poisson effect. Stretched samples were either heated while being stretched or stretched without heating. If the sample is not heated during stretching, the polarization dependence vanishes after shape recovery, while polarization-dependent optical properties remain for samples heated during stretching. Simulations of the polarized optical responses of Au NP dimers at different distances are consistent with experimental results and allow estimation of the average interparticle spacings.

Shape Memory Effect on Plasmon Coupling in Shape Memory Polymers with Embedded Gold Nanoparticles

by
Prachi Rajendra Yadav

A thesis submitted to the Graduate Faculty of
North Carolina State University
in partial fulfillment of the
requirements for the degree of
Master of Science

Materials Science and Engineering

Raleigh, North Carolina
2018

APPROVED BY:

_____	_____
Dr. Joseph B. Tracy Committee Chair	Dr. C. Lewis Reynolds
_____	
Dr. Michael Dickey	

DEDICATION

I want to dedicate my work to my family for showing how unwavering support and empathy help a person pass tough times and come out stronger. I also want to dedicate this work to Dr. Joseph Tracy for being the perfect mentor I needed and teaching me the value in perseverance.

BIOGRAPHY

Prachi Rajendra Yadav was born on 22nd of May 1993 in Rahimatpur, India. She studied electronics and telecommunication engineering in the University of Pune, India and completed the Bachelor of Engineering degree. She came to NC State in 2015 for her masters in Nanoengineering and worked in Dr. Joseph Tracy's group. After completing masters in Nanoengineering in May 2017, she joined the master's program in Materials Science and Engineering department at NC State.

ACKNOWLEDGMENTS

I would like to thank my advisor, Dr. Joseph Tracy and the Tracy research group for their guidance. I want to thank Edna Deas, Dr. Lewis Reynolds, Dr. Michael Dickey and Dr. Elizabeth Dickey for their support in academic and administrative tasks. I want to thank the members at AIF and other facilities at NC State who have helped greatly with my work. And, it is important to mention my thanks to Dr. Amy Oldenburg to help with simulations to make my work complete.

TABLE OF CONTENTS

LIST OF TABLES

Chapter 5: Shape Memory Effect on Plasmon Coupling in Shape Memory Polymers with Embedded Gold Nanoparticles

LIST OF FIGURES

Chapter 1: Introduction to Gold Nanoparticles

1.1. Overview of Nanomaterials

Materials with at least one dimension on the nanometer scale (up to ~100 nm) are called nanomaterials. These materials can be classified as 0D, 1D, and 2D nanostructures according to number of nanoscale dimensions. 3-D bulk structures can be made from these materials. Figure 1.1 shows examples of 0-D to 3-D nanomaterials and respective variations in the density of states, $g(E)$. Due to their unique physical and chemical properties, nanomaterials have been studied extensively for numerous applications, including electronics to medicine, agriculture, and energy.

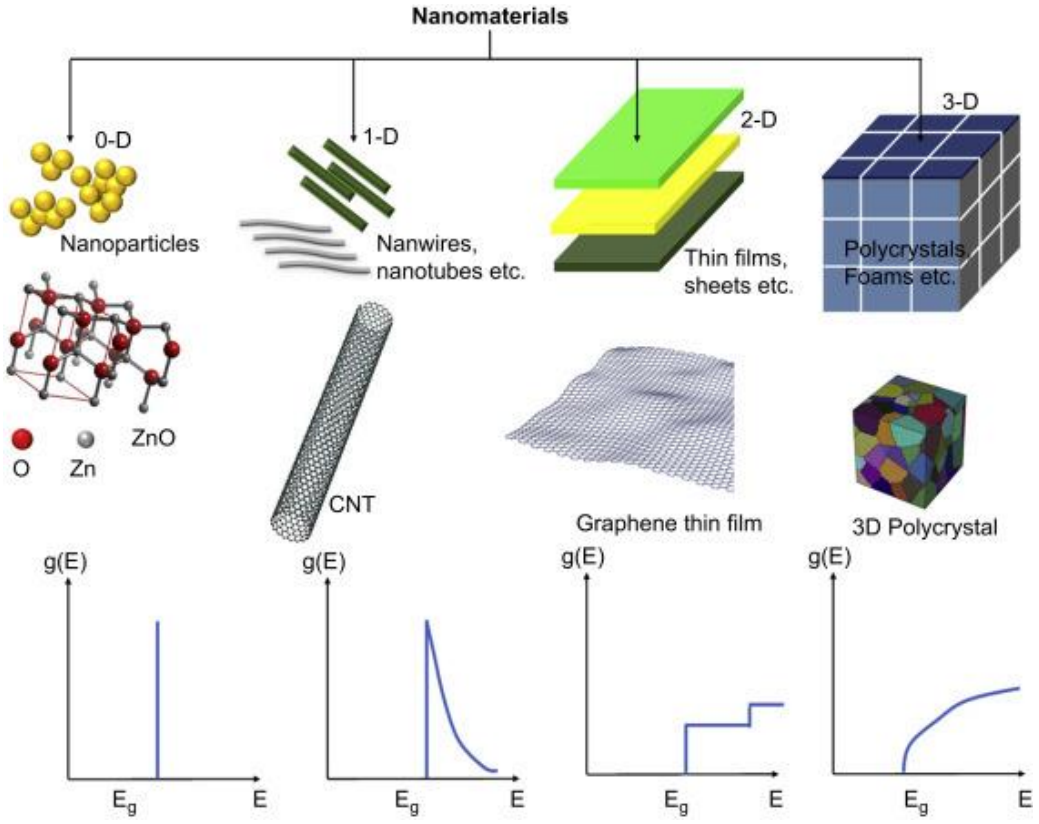

Figure 1.1: Classification of nanomaterials[1]

Nanomaterials exist in nature, and there have also been manmade nanomaterials from centuries before. The latter is evident from the examples of unintentional nanotechnology

discovered in examples like strength enhancement of sword blades,[2] nanostructured pigment in Maya blue,[3] and stained glass, such as the Lycurgus cup and in some churches.[4, 5] With advances in synthesis and materials characterization techniques, nanoscience and nanotechnology in nature became an active area of research to inspire the design of advanced synthetic products. The examples in nature have inspired researchers to use nanomaterials and structures for numerous applications. For example, gecko-inspired nanostructures on the surfaces of polymers have been shown to enhance their shear adhesion and hydrophobicity. Another bioinspired example is micro-optical implants used for sensing intraocular pressure based on longtail glasswing butterflies. Examples of application of bioinspired nanostructures for robotics applications include actuation of bacterial flagella structure modified by attaching superparamagnetic NPs and optically actuated microswimmers inspired by phototaxis of motile photosynthetic microorganisms.[6-9]

1.1.1. Approaches for synthesis of nanomaterials

Methods for synthesizing nanomaterials can generally be classified as top-down or bottom-up approaches. In the top-down approach, the desired structure is obtained by removal of unwanted parts of a bulk parent material. This is a subtractive method of synthesis. The bottom-up approach, in contrast, involves nucleating and growing nanomaterials from smaller, molecular precursors. In both the approaches, matter is subtracted or added with respect to physical constraints of or applied to the system and chemicals used in synthesis. An example of the top-down approach is combining photolithography followed by etching to transfer patterns into semiconductor wafers. Using sophisticated processes, the final structure can be as small as ~10-20 nm. Self-assembly is an example of bottom-up approach. The physical and chemical environment around the seed material guides the growth of added material into desired structure. Hybrid approaches can also be designed to take advantage of both subtractive and additive methods. For example, a template can be

fabricated by lithography and self-assembly can be used to patterned material on or within the template.[10]

1.2. Colloids

Colloids are heterogeneous mixtures of particles suspended in a solvent. Nanoparticles (NPs), including Au NPs, are commonly synthesized as colloids dispersed in solvents, which also facilitates their surface functionalization and assembly. Due to the small size of the Au cores and stabilization by coating around the particles, they can be designed to minimize aggregation and remain dispersed in solvents for long periods of time.[11] Some applications of colloidal NPs are:[12-14] PEGylated Au NPs are used in targeted treatment of cancer; magnetic NPs in MRI as contrast agents with low toxicity, which can also be functionalized for targeting and can be employed in therapy as well as diagnosis.

1.2.1. Synthesis and Functionalization

Au NPs can be synthesized with controlled sizes and shapes and can be further tailored by surface functionalization for different applications. A common method for forming Au NPs is addition of a chemical reducing agent to an Au salt, which drives nucleation and growth. For anisotropic growth, such as nanorods, specific reactants are used that promote crystal growth from the seeds along a certain crystal direction. For spherical NPs, the reactants promote growth uniformly in all directions.

The first documented instance of colloidal Au formation is from Faraday. He studied optical properties of thin films of Au obtained by chemically etching Au leaf. From this etching process, he observed a ruby-colored liquid, which was Au NPs.[15]

Turkevich et. al. developed and investigated several methods for synthesizing colloidal Au, including a widely used citrate reduction method. They also described the processes of nucleation

and growth of Au NPs. Reduction of ionic Au to Au(0) drives nucleation. Their work compared colloidal Au formed by several methods, including Bredig's electric arc method and reduction of $HAuCl_4$ with different reducing agents. They also postulated laws governing nucleation and growth mechanisms.[16] Frens studied the effect of the rate of nucleation on the size distribution of the synthesized Au NPs. Varying the amounts of the reactants changed the rate of reduction, which resulted in changes in the NP size.[17] Furthermore, in 2006, Plech et. al. reported variations to this method by using employing UV light at room temperature and investigated how the reaction conditions affect the growth of Au NPs. Small clusters of a few nm in size grow into larger NPs through coalescence of their cores.[18] For Au NP synthesis following the Turkevich method, a four-step growth mechanism (Figure 1.2) was reported by Polte et. al. First, reduction of the precursor drives formation of small clusters, followed by coalescence of clusters, then growth by diffusion, which continues until the Au precursor has been completely consumed.

Growth of Au NPs using stronger reagents is slightly different, because reduction occurs more quickly, resulting in a higher concentration of metal monomers during reduction and followed by growth due to coalescence and aggregation.[19]

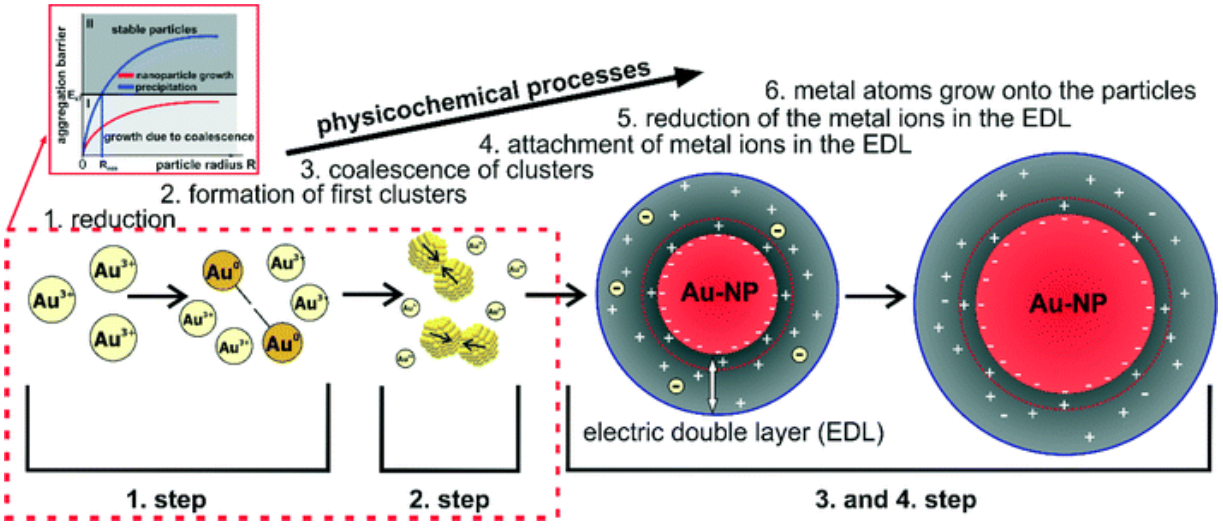

Figure 1.2: 4-step nanoparticle growth in Turkevich method[19]

Wilcoxon et. al. demonstrated a novel method of Au NP synthesis using reverse micelles, which is distinct from the previously reported aqueous synthesis processes. Au salt added to the surfactant/solvent mixture that forms inverse micelles is reduced when a reducing agent is added, driving nucleation and growth of Au NPs within the inverse micelles. The surfactants then serve to stabilize the Au NPs as colloidal dispersions.[20] Due to non-aqueous solvent, the NPs can be used for processing or applications, where stability in an organic solvent is desired. The size of the Au NPs can be adjusted by varying the reaction conditions, including temperature, concentration, and reactants.

Brust et. al. developed a widely used biphasic (water-toluene) method of thiol-based synthesis and functionalization of Au NPs. This method gives NPs with thiolates on the surface, which can be further modified, displaced via ligand exchange, and serve as a basis for several applications.[21] This study was followed by a related single-phase (organic) synthesis of thiolate-stabilized Au NPs.

Hiramatsu et. al. developed a method for synthesizing organoamine-protected Au and Ag NPs.[22] This method is simple, reproducible, and produces NPs with low size polydispersity. The reaction mechanisms of Au-amine complexes were studied by Gomez et. al.[23]

1.3. Properties of Au

Au is employed in a range of applications, despite its cost, due to its physical and chemical properties.[24-26] Bulk Au is malleable, ductile, conductive, rather chemically inert, and can be alloyed. The electronic structure of bulk Au is responsible for its interband transition (5*d* to 6*s*) at ~2.4 eV, which gives bulk gold its characteristic color.[24]

Gold, a transition metal, can donate or accept electrons and has variable valency. Au(-I) compounds are formed when Au accepts electron and acquires anionic character. Au(0)

compounds are of the form of Au clusters. The clusters can have a single Au atom nucleus, or homogenous multi-Au-atoms nucleus, or heterogenous multi-Au-metal-atoms nucleus. Also, compounds with Au(I), Au(II) and Au(III) can be synthesized with corresponding chemistry.[24] The optical properties of metals were studied by Garnett.[27] Later Goad et. al. explained the surface plasmon resonance (SPR) for colloidal metal particles.[28] The SPR is the origin of many interesting properties of noble metal NPs and is discussed in more detail in Chapter 2. Au nanomaterials can be synthesized in form of clusters, nanospheres, nanorods, nanocages or nanomaterials coated with another material. These materials have distinct optical and catalytic properties. These materials absorb and scatter part of the electromagnetic spectrum depending on their composition, size, and shapes and can thus appear different colors in dispersions. The shape-tunable optical properties of Au NPs are useful for medical diagnosis and cancer therapy. NPs can also be functionalized and modified (e.g. encapsulation with polymers) to control their properties for specific applications.[29] Another interesting property is the core size and ligand thickness dependence of the electrical conductivity of alkanethiolate-stabilized Au clusters.[30] Heterogeneous Au NPs formed by covering Au nanospheres with vanadium dioxide (VO_2) undergo a blueshift in their SPR, which is reported to be an effect of semiconductor-metal transition of VO_2 at 67 °C.[31] Imaging techniques like surface plasmon spectroscopy (SPS) and surface enhanced Raman spectroscopy (SERS) are enhanced using NPs and their plasmonic properties.[32-35]

The catalytic properties of Au NPs are also of widespread interest. Despite the rather noble nature of bulk Au, Au NPs are much more catalytically active and have been applied in heterogeneous and homogeneous catalysis.[24] The reactivity of Au with hydrogen, and its role as a catalyst in oxidative dehydrogenation and in isomerization of hydrocarbons is reported by Bond.[36]

Early evidence of catalysis by Au NP was for oxidation of CO.[37] Haruta also reviewed the catalytic properties of Au in bulk and nanoparticulate forms.[38]

1.4. Characterization

Some common techniques for characterizing the structure, size, and optical properties of Au NPs are summarized below.

Transmission Electron Microscopy (TEM): The size and shape of NPs can be imaged by TEM, which provides 2D images, though tomography is a more specialized technique that gives 3D images. TEM is commonly used to measure the size and size distribution of NPs.[39]

Scanning Electron Microscopy (SEM): Like TEM, SEM utilizes electrons for imaging, but the images in SEM are formed by electrons scattered by the sample and not by the transmitted electrons. Surfaces of thick samples can be studied using SEM, unlike TEM, which requires transmission of electrons through the sample.[40, 41]

Optical absorbance spectroscopy measures the light transmitted through a sample and is commonly used to characterize the SPR of plasmonic NPs. Depending on the size, shape and surrounding medium, plasmonic metal NPs show strong optical absorbance at specific wavelengths. The SPR and interactions of plasmonic NPs with light are discussed in more detail in Chapter 2.

Small Angle X-ray Scattering (SAXS): The pattern of X-rays scattered by the sample at small angles is measured, which yields information about the structure of the sample. SAXS measurements can give information about size of NPs and their arrangement within a sample.[39]

Chapter 2: Plasmon Coupling and Gold Nanoparticles

2.1. Surface Plasmon Resonance

For lower frequencies of electromagnetic (EM) waves (up to visible spectrum), metals are opaque and appear shiny. They absorb light and reemit in form of reflection. For frequencies in near-infrared and visible spectrum, the EM field can penetrate deeper into the metal, but is still attenuated by absorption and also scattered or reflected. At still higher frequencies (UV spectrum), the metals act as a dielectric medium.[42] These interactions of metals with light depend on the electronic structure of the metal, which for nanoparticles, depends significantly on their size and is discussed further below.

Plasmons are quanta of electron oscillations. Light incident on planar metal-dielectric boundaries at a certain angle of incidence is absorbed and drives excitation of the conduction electrons in metals, causing displacement of these electrons from the remaining cationic cores, creating an electric dipole. These excitations are termed surface plasmons. The displaced electron clouds experience restoring Columbic forces due to attraction from the positive nuclei and thus begin to oscillate when driven by the incident EM field. This phenomenon is known as the surface plasmon resonance (SPR), which occurs at the frequency where the light and restoring oscillations are strongly coupled. These oscillations propagate along the planar interface at the surface of the metal in the form of surface plasmon polaritons (SPPs).[42-45]

SPP propagation is affected by the dimensions of metal and dielectric, resulting in significant differences for metal films and nanoparticles (NPs). In NPs, the SPR phenomenon is confined to nanoscale, localized, non-propagating oscillations of electrons, which is known as the localized surface plasmon resonance (LSPR). The LSPR is the origin of the unique colors in plasmonic NPs, which differ from material to material, and the LSPR enhances the absorption and

scattering of light by plasmonic NPs. When light is absorbed by the NPs corresponding the LSPR, electrons in the conduction band become excited, creating an electric dipole with respect to the positively charged core of the NP. The amplitude of displacement depends on the frequency of the incident light. The displacement is maximized when the incident frequency matches the plasma frequency, which is the resonance condition. Figure 2.3(a-b) depicts surface plasmons at a metal-dielectric planar interface and in metal nanoparticles. The oscillations are damped by collisions of the electrons in scattering processes, such as electron-electron scattering, electron-photon scattering, electron-defect scattering, and electron-surface scattering. Damping affects the absorption of light and thus affects the optical absorption spectrum, often as a broadening of the LSPR peak.[46, 47]

The medium surrounding the NPs also affects light absorption, which is briefly discussed in Section 1.2. The sensitivity of the LSPR in response to the dielectric constant of the environment has been applied for biosensing.[48]

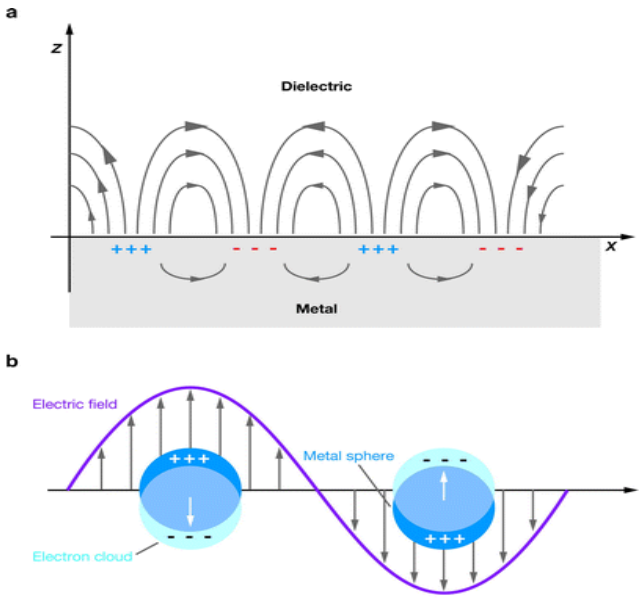

Figure 2.1: (a) SPR in metal-dielectric planar interface, (b) LSPR in spherical plasmonic metal NPs[49]

Since plasmonic NPs absorb and scatter light, optical property measurements are a commonly used characterization technique. In optical absorbance spectroscopy, the light that is not transmitted due to absorption and scattering processes is measured, as follows. In a dispersion of *N* NPs, the change in intensity (*I*) over path length (*x*) is given as:[42]

$$\frac{dI(x)}{dx} = NC_{ext}I(x)$$

Here, C_{ext} is the extinction cross-section of a NP, which depends on the complex dielectric function of the surroundings.

$$C_{ext} = \frac{24\Pi^2 R^3 \varepsilon_m^{(3/2)}}{\lambda} \frac{\varepsilon''}{(\varepsilon' + 2\varepsilon_m)^2 + \varepsilon''^2}$$

where $\varepsilon_m$is the dielectric constant of surrounding medium; ε is the complex dielectric constant of metal NP of radius R with real (ε') and imaginary parts (ε''). λ is the wavelength of incident light. From above equation, the absorbance (*A*), which is also known as the extinction, can be quantified as:

$$A = \log_{10}\frac{I_0}{I(x)} = \frac{NC_{ext}x}{2.303}$$

I_0 is the intensity of incident light.

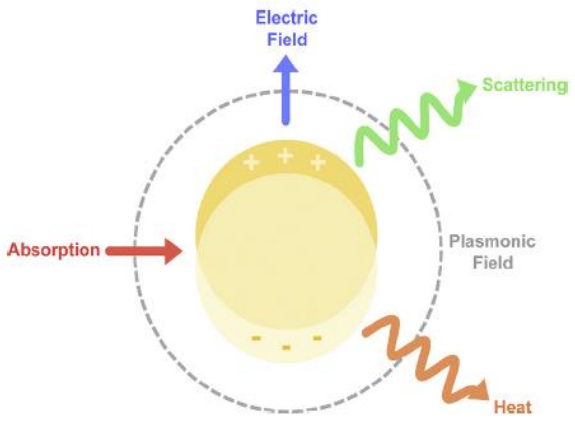

Figure 2.2: Illustration of LSPR in Au NP[50]

Figure 2.4 depicts the absorption, scattering, and heat dissipation processes that occur in the NP when the LSPR is excited.

2.2. SPR and NP shapes and sizes

The theory of interaction of light with spherical particles was developed by Mie using Maxwell's equations by in 1908. Solutions to Maxwell's equations for arbitrary non-spherical shapes can be found by approximating the exact solutions to shapes like spheroids and infinite cylinders.[51] The SPR of NPs also depends on their distribution and concentration within a system, which is reflected in the optical absorbance spectrum.[44]

The modes and frequency of the electron oscillations causing the SPR and associated extinction are affected by many factors, including the shape, size, and composition of the NPs and their environment. In particular, wavelength shifts in the optical absorbance spectrum can be used to assess changes in the environment or state of agglomeration of the NPs, which can also often be reversible.[52, 53]

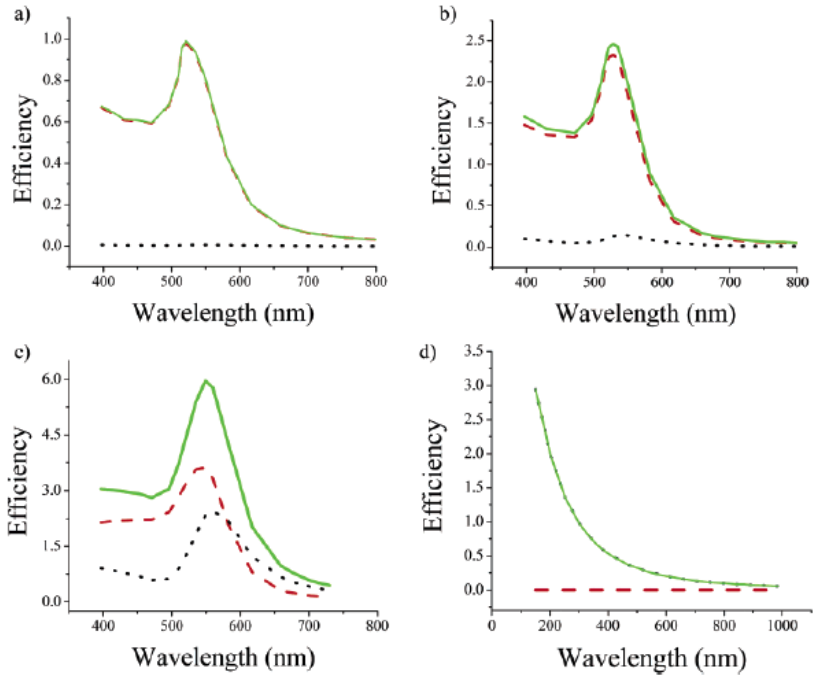

Figure 2.3: Absorption (red), scattering (black), extinction (green) efficiency for Au NPs with diameter (a)-(c) 20 nm, 40 nm and 80 nm, respectively (d) 300 nm polystyrene NP[54]

If the NP size is much smaller than the wavelength of incident light (smaller than ~40 nm), absorption dominates over scattering. For NPs larger than ~40 nm, the contribution of scattering to the extinction is often substantial.[50] Figure 2.3 shows simulations of extinction spectra for spherical Au NPs of three different sizes dispersed in water and compared with polystyrene nanospheres. The effect of particle size for same material can be seen in Au NP spectra.

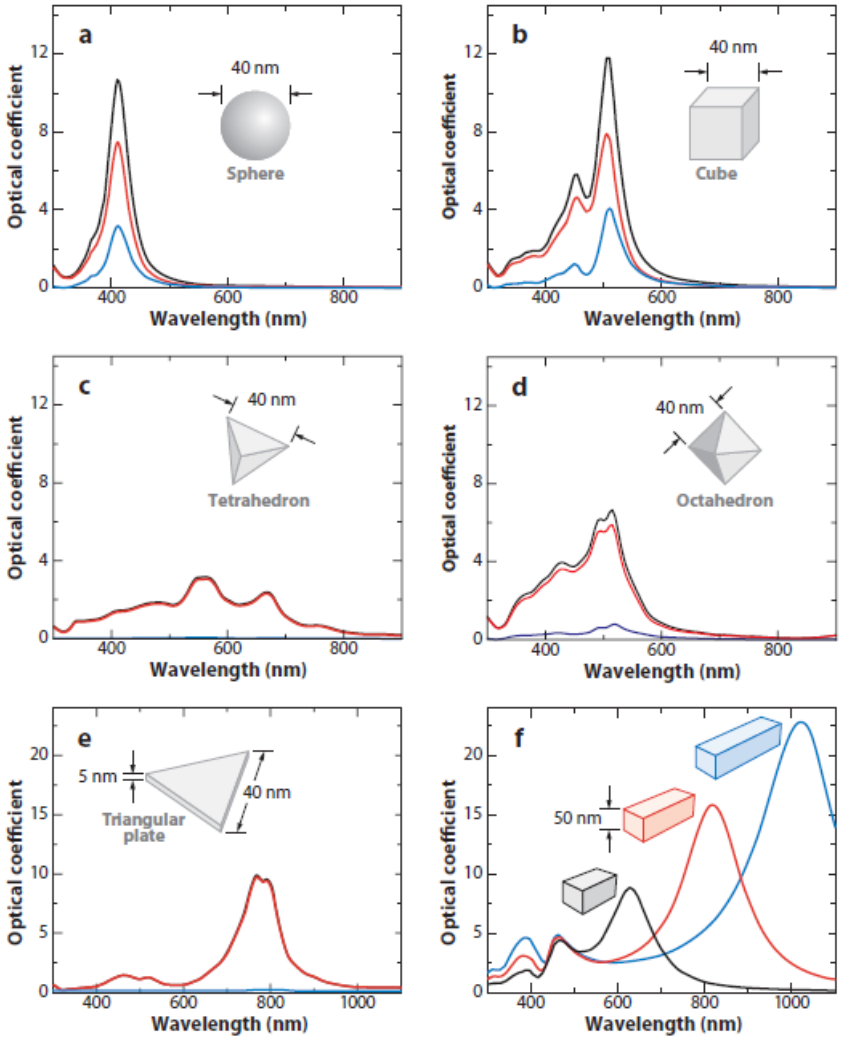

Figure 2.4: Absorption (red), scattering (blue) and extinction coefficients of Ag NPs with different shapes and sizes[55]

For a non-absorbing surrounding dielectric medium, the SPR is redshifted and blueshifted for media with higher and lower refractive index (n_m), respectively. The dielectric function is related to refractive index of medium as $n_m = \varepsilon_m^{1/2}$. Based on the Drude model for the electronic structure of metals, n_m is related to the wavelength of maximum optical absorbance λ_{max} (for visible and infrared frequencies) as:[56]

$$\lambda_{max} = \lambda_p \sqrt{2n_m^2 + 1}$$

where, λ_p is the wavelength at plasma frequency of bulk (ω_p). It is also important to note that the real part of NP dielectric constant is a frequency (ω) dependent quantity($\varepsilon' = 1 - \frac{\omega_p^2}{\omega^2}$), and at resonance, $\varepsilon' = -2\varepsilon_m$.

Plasmonic NPs in the form of composite nanostructures can exhibit altered optical properties, in comparison to bare NPs. If the surrounding medium absorbs light, such as for Au NPs embedded in a graphene matrix, the extinction of light can be affected significantly. For example, the optical absorbance in the SPR region of plasmonic Au NPs is almost completely quenched by the surrounding graphite material.[57] In another study, simulations of the optical absorbance of plasmonic NPs placed on or embedded in graphene in several configurations also reported significant effects of coupling on the optical absorbance.[58, 59] Such composite structures could be in form of NPs embedded in polymers, layers of different materials physisorbed or chemisorbed, coating NPs with different materials or dispersing them in media that promote organization of the NPs within them, or dimers or trimers of NPs.[60-62] Functionalization of NPs can affect the HOMO-LUMO (highest occupied molecular orbital - lowest unoccupied molecular orbital) gap or have an effect on localization or delocalization of HOMO. This induces changes in NP-light interactions, which is observed as a shift in the LSPR and changes in the breadth of absorbance spectra.[52, 63, 64] Malola et. al. have shown the effect of the change in metal core size in

thiolate-stabilized Au-clusters and its effect on the LSPR.[65] Functionalization can also affect plasmon damping by chemical interface damping, in which the LUMO of adsorbates transfers electronic charge from excited metal NPs.[66] As a further example, in the application of Au NPs functionalized with neutravidin coupled to Au thin films for detecting cancer biomarkers, the core size of the Au NP is important for determining the sensitivity of the sensor.[67] The ambient temperature and pressure can also affect the SPR.

2.3. SPR in Au and plasmon coupling

Au NPs are plasmonic metal NPs that can be synthesized in form of spheres, rods, stars, shells, cages, and composite forms consisting of multiple NPs, potentially using different materials. Au nanospheres have a single absorption band depending on their size, whereas anisotropic particles like Au nanorods have longitudinal and transverse absorption bands, and the wavelength of the longitudinal SPR depends on the aspect ratio of the nanorods. Due to their biocompatibility and stability, Au NPs are of interest for many medical applications.[68, 69]

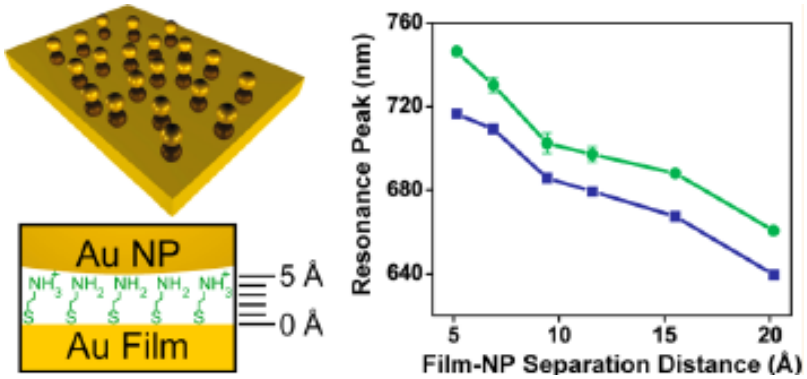

Figure 2.5: Plasmon ruler based on interdependence of film-NP separation distance and corresponding resonance peak[70]

Plasmonic particles placed near one another interact electromagnetically, resulting in coupling of their SPRs. Such plasmon coupling can enhance the magnitude of the localized SPR effect.[71] When two NPs couple forming a plasmonic dimer, they are in a bonding plasmonic mode,

which means the SPR is redshifted to lower energy.[72] Self-assembly of NPs a powerful way of tuning the interparticle distances and obtaining new optical properties. One of many studies reports temperature-responsive hybrid nanostructures, in which temperature controls the coupling between Au NPs.[73] Such distance dependent properties of SPR and plasmon coupling can calibrated with the interparticle distances, allowing for them to be applied as "plasmon rulers".[61, 70]

The absorbance spectra of Au NPs typically undergo redshifts as a result of decrease in interparticle distances.[74, 75] For example, Au NPs have been employed in a plasmon ruler for studying changes in the assembly of DNA. Two Au NPs are initially separated by a DNA strand such that despite the flexible structure of DNA, the interparticle distance is large. When the DNA is caused to buckle, the reduced interparticle distance is detected as a redshift in the SPR of the coupled Au NPs.[72]

Chapter 3: Self-Assembly of Nanoparticles

3.1. Overview of Self-assembly

Self-assembly occurs, when individual components dispersed in a fluid medium spontaneously assemble into an organized structure. In self-assembly, as a bottom-up approach of synthesis, the final structure can consist of almost all the parent material, and loss of material to erosion, etching and related subtractive manufacturing methods can be minimized. Another interesting characteristic of self-assembly that makes it a preferred route of material synthesis over top-down synthesis in some cases is the flexibility offered by tuning chemical and physical components of a given system. This chapter describes different types of self-assembly and their applications in forming complex materials, with a focus on polymer nanocomposites.

Self-assembly is a bottom-up approach for synthesizing nanomaterials, in which molecular precursors assemble into larger systems.[76] Self-assembly of NPs can be triggered by a range of environmental stimuli. For example, the cores of NPs or their organic coatings exhibiting magnetic, electrical, thermal or chemical responsiveness can be manipulated by triggering respective stimuli. Self-assembly is typically driven by noncovalent interactions (e.g., Coulomb and van der Waals interactions) and intermolecular packing.[77] In many cases, in the absence of kinetic barriers, self-assembly brings the system to a state of equilibrium, at which the arrangement of the NPs becomes static. By changing the conditions of the system, however, the organization of NPs or other constituent parts can be further modified in dynamic self-assembly, and self-assembly can often be reversed by selecting the appropriate environmental conditions. Figure 3.5 shows (a) solvent-induced self-assembly, (b) NP cluster fission by solvent, (c) reversible self-assembly of Au-organosilica particles by ethanol or CTAB, and (d) approaches for dynamic self-assembly.

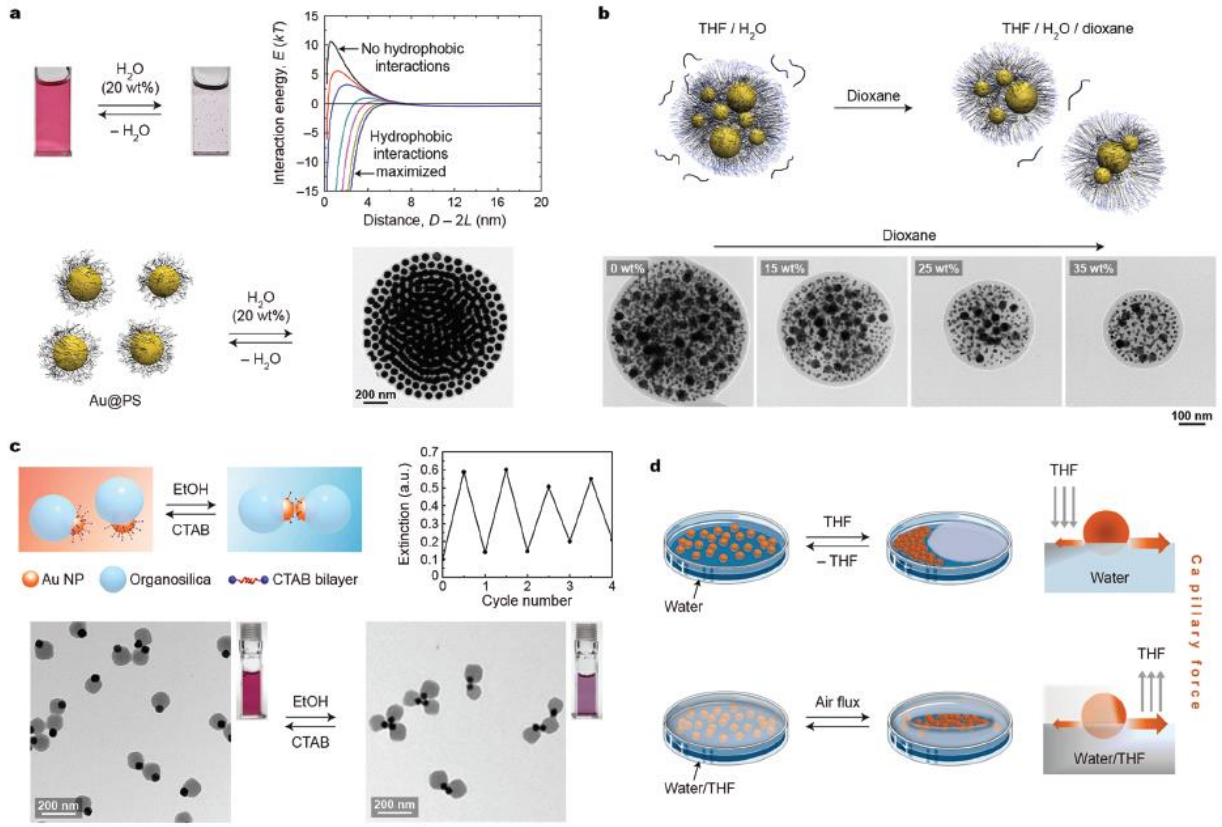

Figure 3.1: Self-assembly driven by different interactions and environmental stimuli [78]

3.1.1. Interactions driving self-assembly

Self-assembly processes are driven by interactions between atoms, ions and/or molecules. Coulomb interactions between charged species and weaker ion-dipole and dipole-dipole, van der Waals interactions can be attractive or repulsive, but repulsive interactions often result in orientation of molecules, followed by attractive interactions. At short distances, electron-electron repulsion dominates, resulting in equilibrium interparticle distances and configurations of NPs that minimize the free energy. These different interactions are manifested in hydrogen bonding, and hydrophobic and hydrophilic interactions that can be used to favor a certain, desired assembled structure.[79] Some examples of self-assembly of NPs include:[80]

1. Hydrogen bonding: Organic coatings on NPs can affect and facilitate self-assembly in two significant ways: Organic coatings can provide sites for hydrogen bonding, thus

causing attraction between NPs. The coatings also cause steric hinderance, which further directs the arrangement of the NPs, particularly the minimum interparticle distances and the local configuration of neighboring NPs. Hydrogen-bonded vesicles and micelles have been shown to form from amphiphiles that can be assembled or dissembled by controlling the pH of the aqueous solution in which these are dispersed.[81]

2. Electrostatic interactions: Charged particles can be attracted to oppositely charged surfaces. Multilayers can be formed by alternating layers with opposing charges, which is the basis of layer-by-layer assembly. For example, oppositely charged derivatives of β-cyclodextrin in water can assemble into dimers.[82]

3. Shape-selective interactions: These are facet-selective attractions that can occur in tetrahedral, octahedral and cubic structures due to geometrical effects and optimization of attractive and repulsive interactions. In biology, receptors and ligands have complementary shapes. Shape selective self-assembly can also be coupled with hydrophilic and hydrophobic patches to guide the assembly process.[83]

4. Hydrophobic interactions: Metal NPs coated with hydrophobic self-assembled monolayers (SAMs) do not disperse in water because they tend to agglomerate due to interactions with the hydrophobic SAMs on adjacent particles. Another example is clustering of polystyrene-stabilized Au NPs with THF as solvent. Hydrophobic interactions can drive the assembly of NPs into clusters.[84] Self-assembly can be subdivided into static and dynamic types. In static self-assembly, a system does not undergo further changes once an assembled structure forms. When a system reaches an equilibrium, static self-assembly is complete. In dynamic self-assembly, a system can undergo further changes with time as

the conditions of the system change. Dynamic self-assembly is common in the molecular biology of living organisms, including the synthesis and function of proteins and DNA.[85]

3.1.2. Classification of self-assembly

Self-assembly can also be classified based on the size of the constituents. For example, molecular self-assembly occurs in atoms, molecules, and crystals on the nanoscale, and meso- or macroscopic subunits can also self-assemble into larger structures. The components, interactions, reversibility, environment and phenomena of mass transport and agitation are all important aspects of self-assembled systems. Adjusting these parameters allows engineering of self-assembly processes. Self-assembly provides routes for making complex 2- or 3-dimensional structures that are inaccessible by top-down methods.[86]

Methods of self-assembly can be further classified based on different aspects of the interactions and the assembled structures formed:[76] 1. Strict self-assembly: a self-assembly process occurs under near-equilibrium conditions and is not kinetically trapped, which facilitates finding the lowest energy state and renders the system sensitive to environmental stimuli. An example of strict self-assembly is the formation of trimetallic double-stranded helicates.[87] 2. Irreversible self-assembly: a series of irreversible reactions leads to formation of self-assembled material, which makes disassembly unlikely without significantly changing the conditions of the system. For example, ovalbumin proteins self-assemble into fibrils with contour lengths increasing as concentration of ovalbumin is increased. But the fibrils thus formed do not undergo change in size (or length) if diluted in water. Thus, the self-assembly of the fibrils is an irreversible process.[88] 3. Precursor modification followed by self-assembly: an inactive precursor is converted into an active form that undergoes self-assembly. As an example, layer-by-layer self-assembly of a nanofluidic diode makes use of this approach.[89] 4. Self-assembly with postmodification: a reversible structure

is formed in a first step, which is then transformed into an irreversible structure. As an example, metalla-supramolecular rectangles were formed via self-assembly in a first step, followed by postmodification to lock this structure was performed. Unmodified rectangles disintegrate in CD_2Cl_2, while postmodification with counterion exchange makes these rectangles robust and stabilizes them against disintegration in CD_2Cl_2.[90] 5. Assisted self-assembly: catalysts and/or external factors that are not a part of the final assembled structure play a role in self-assembly. Molecules or other constituents can serve as chaperones in the self-assembly process by making the environment more conducive to assembly.[91] 6. Directed self-assembly: templates guide the self-assembly process into a particular structure by imposing constraints on the system. For example, the substrate can be templated to make guides for self-assembly by nanoimprint lithography and dip-pen lithography or by patterning grafted polymers on substrates to create chemical patterns. [92] Both biological and non-biological structures can be used as templates to drive self-assembly. Once NPs have been assembled inside or on templates, the templates can often be removed without perturbing the assembled structures.[93] 7. Self-assembly with intermittent processing: a combination of more than one of above categories.

3.2. Self-assembly of nanoparticles in polymers

Composites of polymers and nanomaterials are studied for applications in biomedical devices, flexible electronics, and engineering the mechanical properties of materials.[94-96] For example, Pd NPs can assemble into clusters within poly(2-vinylpyridine), which is guided by the interactions between the NPs and by their interactions with the polymer and the polymer morphology.[97] Two approaches can be used to control assembly of the NPs in the polymer: modifying the environment to alter the polymer morphology, which simultaneously reorganizes the polymer-grafted NPs, or modifying the environment to trigger responses of the NPs.[98] As

further examples, Chen et. al. studied reversible organization of plasmonic Au NPs using triggering of a photo-responsive diblock copolymer.[99] Huebner et. al. also showed a reversible light-induced assembly of Au NPs (grafted to polymer chains) into clusters as azobenzene sidechains in polymer switch from *trans* to *cis* conformations.[100] Assembly of Au NPs dispersed in 2,6-bis(1′-(8-thiooctyl)benzimidazol-2-yl)pyridine (TC8BIP) was chemically controlled by modifying the TC8BIP ligand to control the interparticle distance and annealing the superlattices to form a hcp structure with long-range ordering.[101]

Chapter 4: Gold Nanoparticle – Shape Memory Polymer Nanocomposites

4.1. Shape memory polymer

Shape memory polymers (SMPs) are special class of polymers that can transform from a temporary shape to a preprogrammed permanent shape, thus exhibiting a memory function. The polymer is in a low-entropy state in its undeformed or permanent state and in a high-entropy state after deformation into its temporary shape. The shape memory effect (SME) has been observed in polymers, as well as metal alloys, ceramics and gels.[102] Unlike the case of metal shape memory alloys (SMAs), where the SME is a phase transformation (Figure 4.1), in the case of polymers, it is an entropy-driven phenomenon.[103, 104] SMPs are categorized as chemically crosslinked glassy thermosets, chemically crosslinked semicrystalline rubbers, physically crosslinked thermoplastics, and physically crosslinked block copolymers.[105]

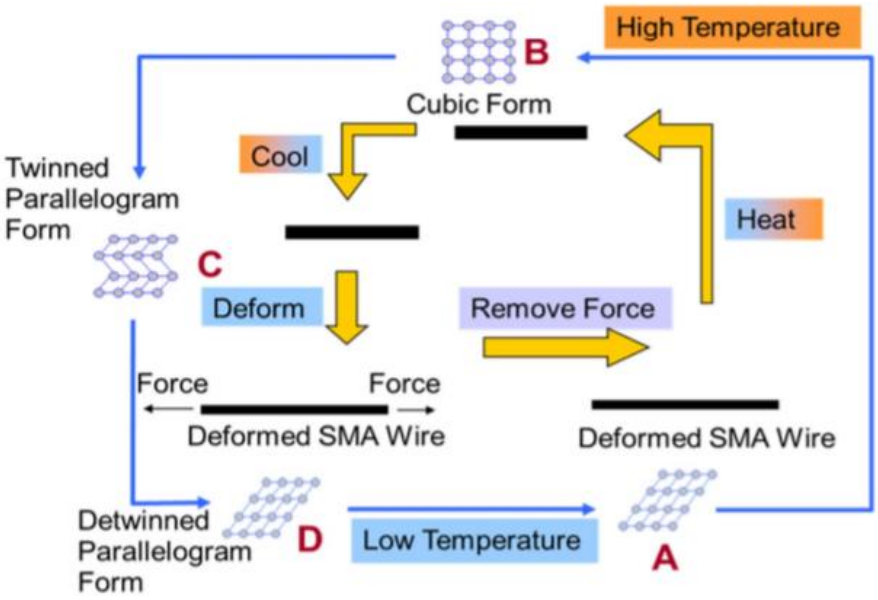

Figure 4.1: SME in SMA[106]

Thermoplastics can be linear or branched chains with strong or weak intramolecular forces.[107]

SMPs have crosslinking and switching segments. Crosslinking segments are responsible for chemical crosslinking between polymer segments through covalent bonding or physical crosslinking as a result of phase separation, hydrogen bonding or physical entanglements between linking segments. The crosslinking density (ν) is related to the elastic modulus (E), universal gas constant (R) and temperature (T) as: $\nu = \frac{E}{3RT}$

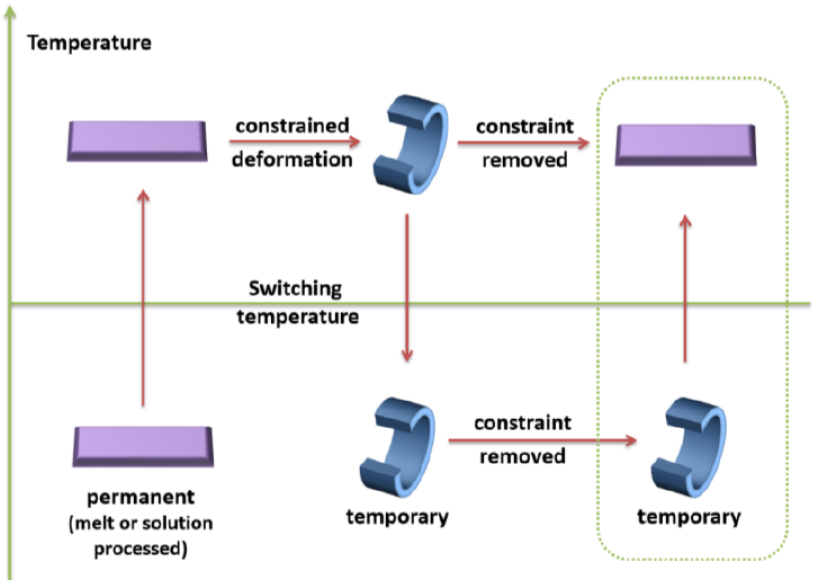

Figure 4.2: Shape memory effect[108]

SMPs with covalently bonded chemical cross links are thermoset SMPs. The crosslinking segment in these softens above the glass transition temperature (T_g), and if temperature is further elevated, it continues to remain soft and then decomposes or burns. Thermoplastic SMPs, on the other hand, are generally block copolymers (BCPs) that undergo physical crosslinking via chain entanglement. These BCPs have a hard segment that undergoes physical crosslinking and a soft or switching segment.

The SME mechanism (Figure 4.2) in SMPs is as follows: After deformation under constraints to set a temporary shape, the switching segments lock it in place. To achieve this, the undeformed polymer in its low-entropy state is first heated above its T_g or T_c (crystallization temperature of soft segment) to a higher-entropy, metastable state. In this second-order phase transition, the polymer transitions from a brittle glassy-state to flowy rubbery-state. The heated polymer can be shaped as desired by applying physical constraints. Upon cooling below T_g or T_c, this shape is locked, and the metastable state of the temporary shape is preserved. When heated unconstrained above T_g again, the polymer returns to its permanent shape, the low-energy state.[109-111] For example, a light-triggered, self-healing and SME has been studied in different polymer and NP composites. Photothermal heating of the exposed area facilitates diffusion of metal into crack of depolymerized metallosupramolecular structure. When light is turned off, cooling locks the new, healed form of the structure (Figure 4.3).[112]

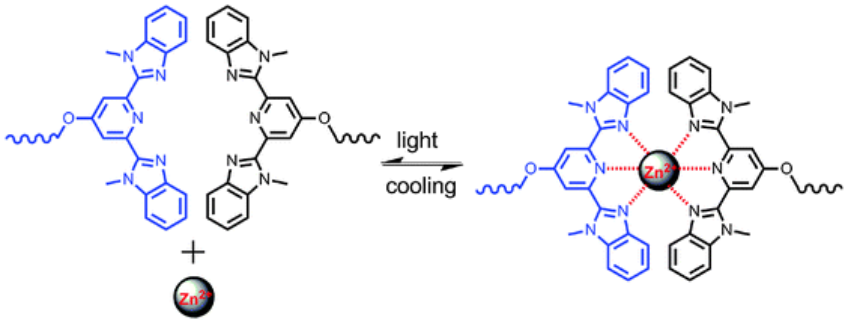

Figure 4.3: Light-triggered self-healing[112]

Magnetic NPs can also induce heating in thermoplastic polymers, triggering shape recovery. In another study, magnetic NPs were embedded in thermoplastic polyetherurethane and biodegradable multiblock copolymers. An AC magnetic field induced heating and increased the temperature up to 88 °C.[113]

Recovery can be driven by direct and indirect heating of the deformed polymer. Direct mechanisms of heating include conduction (with heating elements or apparatus), convection (air

or fluid) and radiation (microwave or IR). Indirect heating mechanisms include induction, Joule heating, laser heating, dispersion in heated environments, (e.g, hot water), photothermal heating and mechanical forces.[111]

4.2. Design and fabrication of composites

Composites consisting of NPs dispersed in polymers have been used in the automotive industry for many years.[114, 115] Reinforcement of polymers with fillers, such as NPs, fibers, clusters, and layered filler material (e.g, silicate nanoclay) can enhance the performance beyond that achievable from a polymer alone.[116] The advantages of dispersing NPs in polymers include the ability to control their placement and assembly within the polymer by controlling the surface chemistry of the NPs, the polymer chemistry, branching, morphology, and the processing conditions.[117] Novel SMP-NP composites can be used in electronics as well as textiles.[118-120]

SMP composites, where the SMP matrix is reinforced with fillers, have been studied extensively.[110] Reinforcing SMPs with fibers, woven CNT mats, cellulose or other material can enhance the mechanical strength (i.e., increased Young's modulus) of the composite material and also strongly affect the optical and thermal properties.[121, 122] Nanoclay particles can improve the SME in composites by causing more complete shape recovery.

Pastoriza-Santos et. al. have reviewed the applications of a wide range of compositions and structures combining plasmonic NPs and polymers, especially for data storage and biomedical imaging and sensing.[117] Two common forms of assemblies of NPs are superlattices or aggregates. An assembled structure with periodic ordering is called a superlattice and if the order is absent, it is called an aggregate. Both superlattices and aggregates of Au NPs can exhibit coupled plasmon resonances.[123] Polymers to which NPs are grafted or are dispersed can serve as spacers between neighboring NPs. The properties of the composites correspondingly depend on the spacing and

interactions between neighboring NPs.[124-127] NPs grafted with polymer chains forming shells around the inorganic cores are termed as "hairy NPs." Adjusting the length of the grafted polymer hairs also allow for control over the NP assembly and thus the properties of the composite. Fernandes et. al. have reviewed this topic extensively.[128]

4.3. Self-assembly of Au NPs in SMPs

There have been several studies of composites combining Au NPs and SMPs. In one study, Au NPs were chemically crosslinked to the surface of a prestrained SMP under tension. Upon heating, the SMP shrinks, and the layer of NPs on the top surface of the film affects the pattern, including the wavelength and amplitude of the wrinkles formed in the shape-recovered films.[129] A poly(ε-caprolactone) SMP with functionalized nanofillers of thiolated cellulose nanocrystal (CNC) carriers with Ag NPs either adsorbed on or grafted to the CNCs were used by Toncheva et. al. to demonstrate fast photothermal heating and shape recovery when triggered by near-infrared light (Figure 4.4).

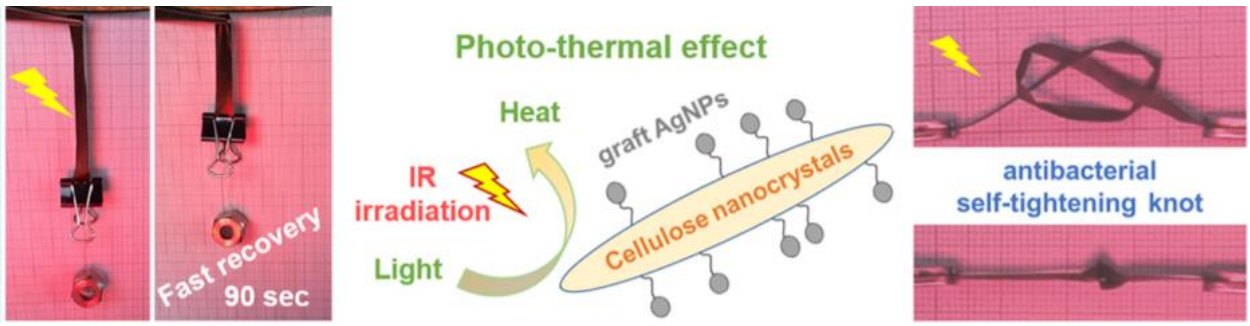

Figure 4.4: (Left) Strain recovery of film with IR light; (center) graphical illustration of composite; (right) SME used to make knot structure[130]

Covalent bonding of the Ag NPs to the CNCs ensures uniform and controlled responses. Strong plasmon coupling is observed in these composites.[130] Application of selective excitation of the LSPR based on the shape and concentration of Au NPs for triggering the SME in SMPs has been reported previously. For example, Mishra et. al. used Au nanospheres and nanorods for

photothermally driven shape recovery of thermoplastic polyurethanes using light-emitting diodes with wavelengths of 530 nm and 860 nm, respectively.[131]

Chapter 5: Shape Memory Effect on Plasmon Coupling in Shape Memory Polymers with Embedded Gold Nanoparticles

5.1. Introduction

This chapter will be submitted for publication with Yadav as first author and is coauthored by Dr. Sumeet Mishra, Dr. Brian Chapman, Dr. Brain Lynch, Dr. Amy Oldenburg and Dr. Joseph Tracy.

5.2. Copy of Manuscript

Introduction

Polymer nanocomposite thin films containing functional nanoparticles (NPs) are a rich and complex system, where the organization of the NPs can determine their properties based on their orientation or coupling.[1-10] When plasmonic NPs, such as Au NPs, are dispersed within or assembled on the surfaces of polymer films, their organization determines the interparticle distances and extent of coupling of their surface plasmons.[11-22] Therefore, nanocomposites based on elastomers and shape memory polymers (SMPs) are of special interest, where there is a capability to alter the spacing between NPs and thereby control the optical properties of the thin film. Plasmonic elastomer and SMP nanocomposites have a potentially wide range of applications, including sensors, optoelectronics, and optical filters.[23-26]

SMPs are a diverse class of polymers with temporary shapes that can be programmed by stretching or shearing. The permanent shape can be recovered by triggering with certain stimuli, most commonly temperature.[27-29] Applying one-way, thermally activated SMPs involves a three-

step process that can be repeated, where the polymer (1) is programmed into a temporary shape via externally applied forces while heating above its transition temperature, (2) cooling below the transition temperature and removing the external forces, which locks the temporary shape at room temperature, and (3) recovery of the permanent shape by heating above the transition temperature. For this study, we have selected a commercially available thermoplastic polyurethane (TPU) polymer, Diaplex MM5520, which has a transition temperature of 55 °C. In a recent study using Diaplex, we showed that photothermal heating of embedded Au NPs can be used to optically trigger shape recovery of bent thin films of the nanocomposite.[30] Here, we have investigated stretching of the same type of film containing embedded Au NPs, with a focus on the optical properties of the thin films and how they change when the film is stretched into a temporary shape and then after heating to return to its permanent shape. As the organization of the Au NPs in Diaplex changes during heating, stretching, and shape recovery, polarization-dependent shifts in the optical absorbance spectra indicate altered coupling of the surface plasmons.

Coupling of the surface plasmons of noble metal NPs is well established for the development of sensors that provide an optical readout of molecular and biological phenomena. Plasmon coupling has allowed for the development of plasmon rulers[31,32] and is employed in surface-enhanced Raman spectroscopy (SERS). In addition to work on polymer composites, there is significant interest in controlling the assembly or aggregation of NPs into clusters and then adjusting the properties of the clusters dynamically with chemical, optical, and thermal stimuli.[33] Use of SMPs for the matrix provides a simple way of mechanically controlling and reversing the assembly of the NPs.

It is well established that stretching polymer films containing embedded plasmonic NPs can impart polarization-dependent optical properties, where spherical and rod-shaped Au and Ag

NPs have been the most widely studied. Shearing during stretching tends to align nanorods with the stretching direction, causing a redshift in the optical absorbance parallel to the stretching direction and blueshift perpendicular to the stretching direction.[22,34-39] Obtaining a polarized absorbance from spherical plasmonic NPs requires that they are have anisotropy in their local environment, such as coupling with other NPs in clusters. The polarized optical response commonly observed for stretching clusters of spherical NPs is a redshift parallel to the stretching direction and a blueshift perpendicular to the stretching direction,[40-43] in agreement with our results, but shifts in the opposite directions have also been reported.[13] The possibility of shifts in either direction could arise from subtle morphological effects determined by the polymer system and the surface functionalization of the NPs. If NPs dispersed within a polymer would be uniformly pulled along with the polymer in the stretching direction and uniformly compressed perpendicular to the stretching direction, then decoupling of the plasmons and blueshifting would be expected when measuring the optical absorbance parallel to the stretching direction, and redshifting would be expected perpendicular to the stretching direction. The reverse trend is usually observed, which may be attributed to microstructural features of the polymer that do not allow uniform movement of NPs, which may effectively pin some of the NPs and then cause them to be pulled into each other along the stretching direction. While the Poisson effect would still occur, compressing the NPs along the perpendicular direction, the more significant result of the stretching and clustering along the stretching direction is weaker plasmon coupling along the perpendicular direction and a corresponding blueshift.

Most previous studies have employed poly(vinyl alcohol) (PVA), which can be stretched but recovery of the initial shape is not possible, and polydimethylsiloxane (PDMS), an elastomer. To the best of our knowledge, the effects of shape recovery of SMPs with embedded plasmonic

NPs on the optical properties of the composite have not been investigated previously. Rather, prior studies of SMPs have utilized the optical properties of the embedded plasmonic NPs to control shape recovery.[30,39,44-50] Use of a SMP matrix enables integration of the polarization-dependent optical properties obtained through shearing with shape memory.

Polarized optical absorbance spectra during stretching of Diaplex indicate a change in the coupling among the NPs. The extent to which the arrangement of the NPs returns to its original state after shape recovery depends on whether the film was heated during stretching. Microscopy after stretching and shape recovery and simulations of plasmon coupling among the Au NPs provide an understanding of the observed behavior. Controlled clustering of NPs in polymer films and the resulting polarization-dependent optical properties suggest that such clusters of NPs can be useful more broadly for transducing macroscale deformation into locally altered properties.

Experimental

Synthesis and Characterization of Gold Nanoparticles. Spherical Au NPs with an average diameter of 17 nm were synthesized according to an established procedure.[51,52] Chemicals used for synthesizing Au NPs included $HAuCl4{\cdot}xH_2O$ (Alfa Aesar, 99.999%, where x was estimated as 3), oleylamine (OA, Sigma Aldrich, ≥98% primary amine), anhydrous toluene (EMD, DriSolv), tetrahydrofuran (THF, EMD, OmniSolv, Non-UV), and methanol (MeOH, Macron, ChromAR). The Au NPs are stabilized by OA and are dispersed in THF after purification.

A reaction solution composed of 24 mL of toluene and 0.6 mL of OA was heated to 120 °C with stirring in a 100-mL round-bottomed flask that was open to ambient atmosphere. A solution of 50 mg of $HAuCl_4$ dissolved in 1.5 mL of toluene and 0.5 mL of OA were added and heated while refluxing at 120 °C for two hours, yielding a red-purple dispersion. The products

were purified by centrifugation after adding a non-solvent to drive sedimentation. 5 mL of the product was mixed with 3 mL of methanol and centrifuged at 3000 rpm (IEC Centra MP4, 816 rotor, 1290 *g*) for 1.5 minutes. After decanting the supernatant, the sedimented NPs were redispersed in THF.

Transmission electron microscopy (TEM) was performed using a JEOL 2000FX microscope by drop casting purified NPs onto to Cu TEM grids with ultrathin amorphous carbon supports. Optical absorbance spectra of solutions and of polymer thin films were acquired using an Ocean Optics CHEMUSB4-VIS-NIR spectrophotometer.

Preparation of Shape Memory Polymer Composite Films. Thin films (~100 μm thick) of Au NPs embedded in a commercially available thermoplastic polyurethane, Diaplex (SMP Technologies, MM5520), were prepared by solvent casting. 0.2 g of Diaplex pellets were dissolved in 5 mL of THF over a period of 2 hours with stirring. A volume of the purified Au NP stock solution containing 6 mg of Au NPs was transferred into an empty vial, and the THF was removed by rotary evaporation. The Diaplex solution was added to the dried Au NPs, which redispersed with sonication. After solvent casting, the Au NPs had a concentration of 3 wt% in the dried Diaplex films. The mixture was poured into polytetrafluoroethylene (PTFE) molds (Savillex 700-925) with dimensions of 10 cm (*l*) × 2.5 cm (*w*) × 2 cm (*h*). Composite NP-Diaplex thin films were obtained after the solvent evaporated for 6-7 hours in a fume hood at room temperature.

Stretching and Characterization of Stretched Films. The films were stretched using a custom-built stretching jig (photograph in Supporting Information, Figure S1) for uniaxial stretching. Films with a length of 6 cm and width of 2.5 cm were cut from the middle of each film, clamped in the jig, and stretched laterally using aluminium grips. Each film was placed with 2 cm from each end within the clamps used to pull each both ends of the film, giving an active length

for stretching of 2 cm. Each film was stretched to 6 cm, a strain ($\Delta l/l_0$) of 2. Four identical films were prepared and stretched and heated under different conditions: (1) control: not heated, not stretched, (2) control: heated, not stretched, (3) stretched with heating, and (4) stretched without heating.

Stretching with Heating. This sample was prepared by placing the jig loaded with the film in an oven under ambient atmosphere at 100 °C. After leaving the unstressed film in the jig in the oven for 10 min to thermally equilibrate and soften the film, the jig was removed from the oven and stretched by 1 cm. After placing the jig in the oven again for 2 min to keep the film warm, the jig was again removed, and the film was stretched by an additional 1 cm. This procedure was repeated two more times, until the film reached a final length of 6 cm. The film was placed back into the oven for 4 min before cooling to room temperature. After cooling, the film retained a stretched temporary shape until shape recovery was driven by heating.

Stretching without Heating. The film was clamped in the jig, as described above. The grip of jig was moved slowly, over a period of 10 min, and in small increments, the film was stretched to a final length of 9 cm. Slow stretching was necessary to prevent the films from fracturing during stretching. The film was intentionally overstretched because it undergoes partial shape recovery upon removal from the jig. The sample was left in the jig for 48 hours prior to removal. The active region of the film retracted to a length of 6 cm within about 4 hours, after which the recovery significantly slowed and minimal changes occurred over several days.

Unconstrained Heating for Shape Recovery. Although the Au NPs in the films can be used to drive shape recovery through photothermal heating,[30] an oven was used in this study to ensure uniform and complete shape recovery. Each of the stretched films was cut along the length into two pieces for further measurements, one that was left in the stretched state, and one that was

heated for shape recovery. For shape recovery, the films were placed, unclamped, in an oven at 80 °C for 15 s, and shape recovery occurred quickly, within the first few seconds.

Characterization. Optical absorbance spectroscopy measurements of the thin films were acquired using an Ocean Optics CHEMUSB4-VIS-NIR spectrophotometer. The thin films were cut with scissors to fit into a glass cuvette, and each film rested against one wall of the cuvette with the stretching direction oriented vertically. For polarized optical absorbance spectroscopy measurements, polarizer films (Edmund Optics 43-781) were cut and placed in the cuvette next to the sample, such that light in the beam first went through the polarizer and then through the sample. The designations parallel and perpendicular indicate the relative orientation of the polarization axis and the direction in which the sample film had been stretched. For polarized measurements, the blank was the polarizer in the corresponding orientation and no sample. For SEM measurements, the samples were mounted to Al holders with double-sided carbon tape. Carbon coatings were applied to all samples to avoid charging. The samples were imaged using a FEI Verios 460L field-emission scanning electron microscope.

Optical Property Simulations. Simulations of the extinction cross section of dimers of Au NPs within a Diaplex matrix were performed using methods described in the Supporting Information. The effects of varying the interparticle distance on the polarized and the unpolarized extinction cross sections were simulated and compared with the experimental results.

Results and Discussion

The experimental results can be understood by considering the mechanical effects of stretching on the organization of the Au NPs. In the as-prepared samples, the Au NPs disperse in Diaplex in small clusters, which is likely caused by the nature of the chemical interactions between

the oleylamine ligands and Diaplex. Diaplex is a block copolymer, composed of hard segments that crystallize, methylene diphenyl diisocyanate, soft segments that have a glass transition temperature of ~55 °C, and a chain extender, 1,4-butanediol.[53] The morphology of Diaplex and related TPUs when strained is complex and has also been investigated.[54] Based on this background, and the general challenge of dispersing NPs within polymers,[55,56] it is not surprising that the Au NPs form clusters within the as-prepared Diaplex films. Prior to stretching, the SPRs between the Au NPs within the clusters are already coupled, based on the optical properties discussed in the next section. The distance between Au NPs within clusters decreases parallel to the stretching direction and increases in the perpendicular direction, because of non-uniformities in the stretching process, which is opposite to the Poisson effect. Consequently, the optical absorbance spectrum undergoes redshifts and blueshifts for light polarized parallel and perpendicular to the stretching direction, respectively. Heating during stretching prevents the composite sample from completely recovering its optical properties because the combination of heating and stretching makes it so that the polymer does not fully recover its shape on the nanoscale, even though it does recover its shape on the macroscale. In contrast, stretching without heating allows complete nanoscale shape recovery.

Optical Characterization. Au NPs disperse in THF and have maximum absorbance at 522 nm (Supplementary Information, Figure S2). After dispersion in the polymer film a blueshift in the maximum absorbance to 539 nm is observed, which is not affected by heating without stretching (Supplementary Information, Figures S3-S4). Prior to stretching, there is no polarization anisotropy. In comparison with the experimental results, simulated extinction spectra of isolated Au NPs exhibit maxima at 520 nm in THF and 533 nm in Diaplex (Supporting Information, Figure S7), where the differences arise from the different refractive indices of THF and Diaplex.

Comparing the simulated peak of 533 nm in Diaplex to the experimental value of 539 nm there is an apparent redshift, which can be attributed to clustering of the NPs in the experiment, which was not modelled in the simulation. Clustering of the Au NPs during preparation of the Diaplex films, resulting in strong plasmon coupling despite the low loading of the Au NPs in the films (3 wt%), is further confirmed by SEM (*vide infra*).

For samples stretched with and without heating, redshifts and blueshifts were observed for light polarized parallel and perpendicular to the stretching direction, respectively (Figures 2a, 3a). A blueshift is only possible because of the clustering of the Au NPs prior to stretching, such that their plasmons are initially coupled. After heating to drive shape recovery, the blue- and redshifts are reduced for the sample that was heated during stretching (Figure 2b) or eliminated for the sample stretched without heating (Figure 3b). These results suggest that heating affects the ability of the composite samples to return to their initial configuration. The wavelengths at the optical absorbance maximum are summarized in Table 1. While some samples exhibit significant shifts in their polarized optical absorbance spectra, the peaks of the unpolarized optical absorbance spectra lie within a narrow window of 536-539 nm (Supporting Information, Figures S3-S6).

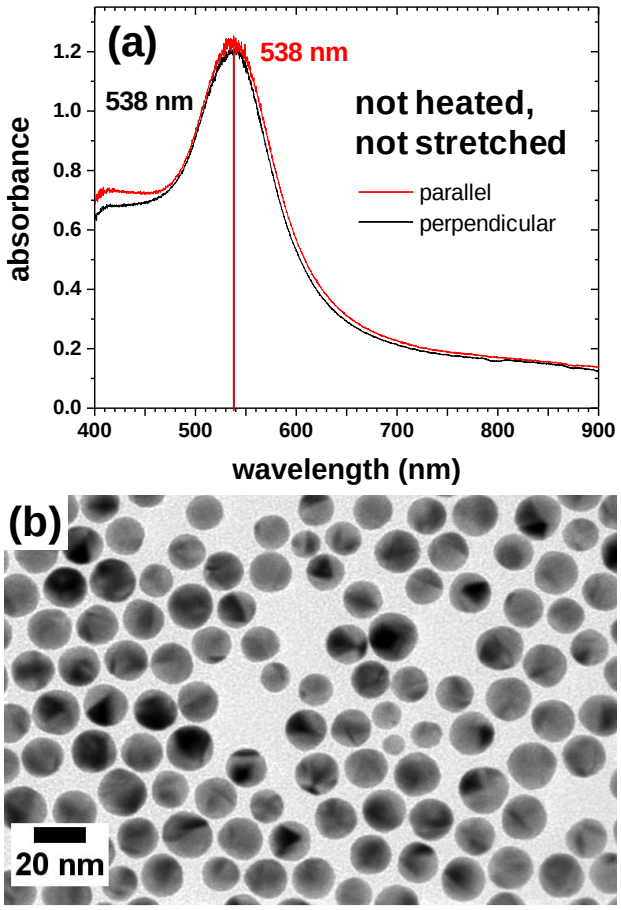

Figure 5.1:(a) Polarized optical absorbance spectra of Au NPs in Diaplex film before stretching or heating and (b) transmission electron micrograph of Au NPs dropcast from tetrahydrofuran for TEM.

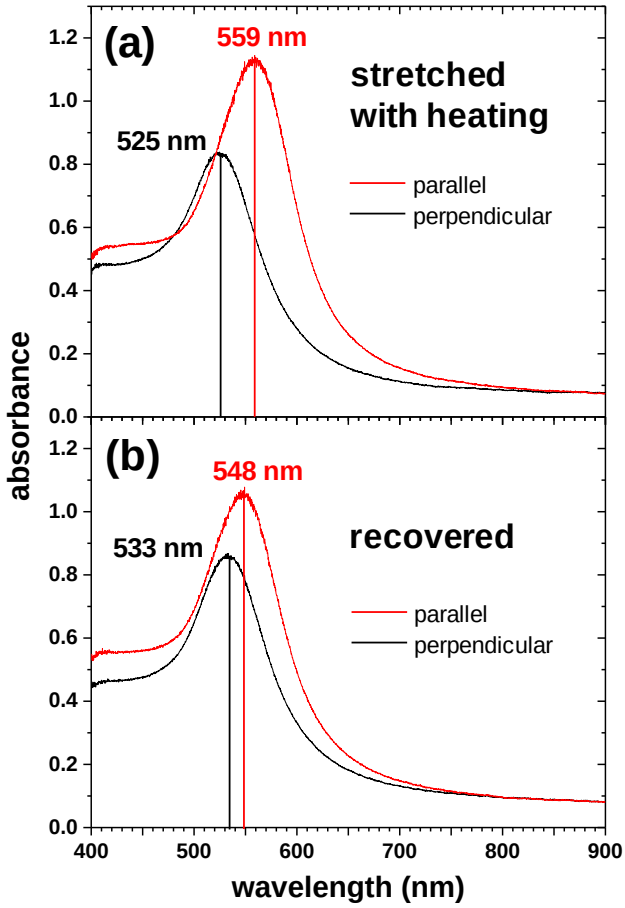

Figure 5.2: (a) Polarized optical absorbance spectra of Au NPs in Diaplex film (a) after stretching with heating and (b) after (a) and heating under zero stress to drive shape recovery.

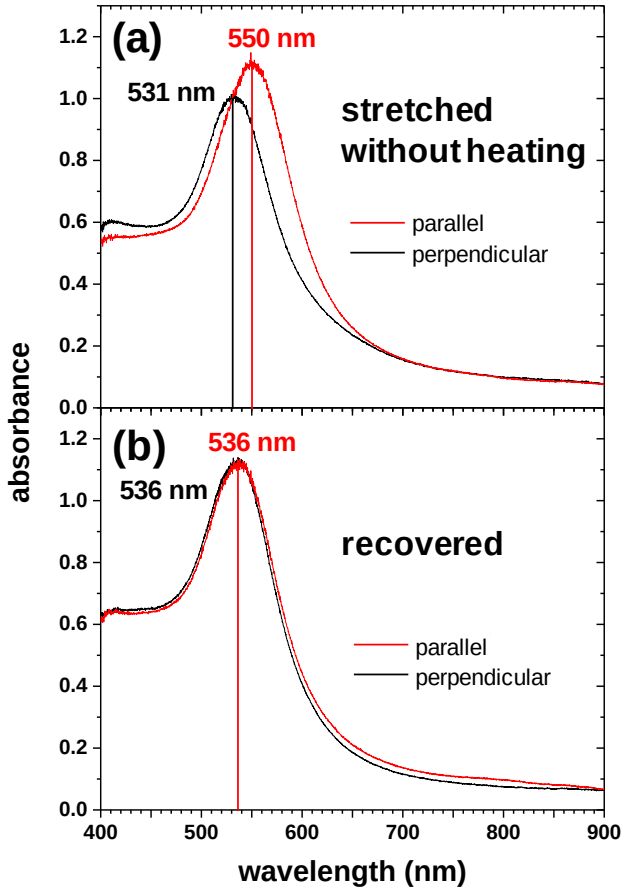

Figure 5.3:(a) Polarized optical absorbance spectra of Au NPs in Diaplex film (a) after stretching without heating and (b) after (a) and heating under zero stress to drive shape recovery.

Table 1. Measurements of peak wavelength in unpolarized (UNP) and polarized (⊥ and ∥) optical absorbance spectra for all samples.

Figure	**Sample**	**1. ∥ (nm)**	**2. ⊥ (nm)**	**3. UNP (nm)**	**Δ(1-2) (nm)**	**Δ(1-3) (nm)**	**Δ(3-2) (nm)**	**Sep[a] (nm)**
1a, S3	Untreated	538	538	539	0	-1	1	>6[c]
2a, S5a	Stretched, heated	559	525	537	34	22	12	3[b]

Table 1 (Continued)

2b, S5b	Stretched with heating, recovered	548	533	538	15	10	5	5[b]
3a, S6a	Stretched without heating	550	531	537	19	13	6	5[b]
3b, S6b	Stretched without heating, recovered	536	536	536	0	0	0	>6[c]
S4	Heated, not stretched	537	537	538	0	-1	1	>6[c]

[a]Average interparticle separation (Sep) between the metal surfaces of Au NPs based on comparison with simulations of dimers of Au NPs.

[b]From comparison with polarized optical absorbance spectra (Figure 5) for stretched samples that exhibited significant polarization effects.

[c]From comparison with unpolarized optical absorbance spectra (Supporting Information, Figure S8) for unstretched samples that did not exhibit polarization effects. At wavelengths below ~540 nm, corresponding to interparticle separations exceeding 6 nm, the sensitivity of the peak wavelength to the interparticle separation distance is diminished.

Structural Characterization. Imaging these samples by scanning electron microscopy (SEM) is challenging because of charging, and there are is some variability among the images of different regions within the same sample. This suggests that the distribution of the initial clusters may be sensitive to some variables of film preparation that were not controlled here, such as the evaporation rate and the amount of excess oleylamine present with the Au NPs. Nevertheless, some general observations by SEM are important. In a control sample prior to stretching or heating (Figure 4a), many of the Au NPs are present in dimers or small clusters. There is a distribution of arrangements, which would be expected to cause differences in plasmon coupling among Au NPs. This would be expected to lead not only to redshifting during dispersion in Diaplex, already discussed above, but also to broadening of the SPR peak, which is apparent in the unpolarized

optical absorbance spectra, Supporting Information, Figures S1, S2b. An important caveat for all of the SEM images is that they are two dimensional, and information about the arrangement of the NPs in the out-of-plane direction is limited.

After stretching with heating (Figure 4b), more of the clusters appear to be aligned parallel to the stretching direction, which is consistent with shearing during stretching. After shape recovery (Figure 4c), alignment of the clusters along the stretching direction is diminished or vanishes. While polarized optical absorbance spectroscopy shows a persistent polarization effect after shape recovery, the local structures causing this effect are too subtle to be directly observed by SEM, which is why we have also performed optical property simulations to get a more detailed understanding.

Two types of regions were observed for the sample stretched without heating that persisted after shape recovery, relatively dispersed regions with minor clustering (Figure 4d,e) comparable to the unstretched sample and the sample stretched with heating, and regions with larger agglomerates (Figure 4f,g). Microscale cracks also formed perpendicular to the stretching direction (Figure 4f). Within the agglomerates, the Au NPs formed chains and had gaps between them, aligned with the vertical direction. Despite the structural heterogeneity of the sample stretched without heating, the polarized optical properties show no polarization effect after shape recovery, which implies that neither type of structure causes polarization effects after shape recovery.

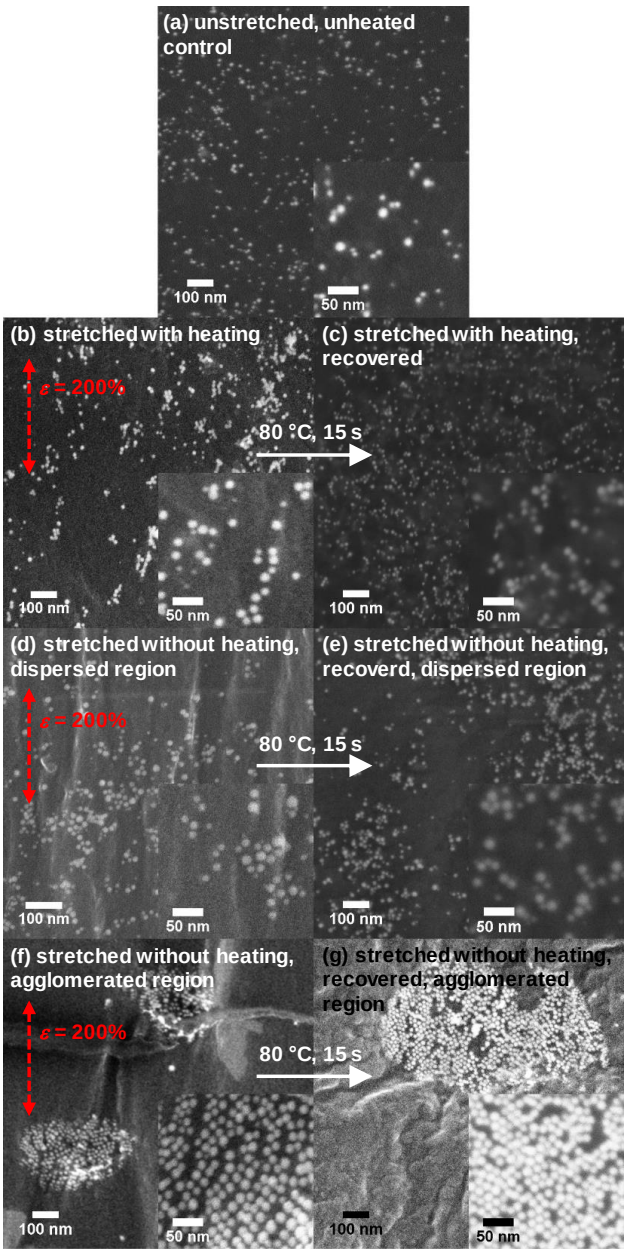

Figure 5.4: SEM images of (a) unstretched, unheated control sample, samples stretched with heating (b) before and (c) after recovery, two types of regions in samples stretched without heating before recovery, (d) dispersed and (e) agglomerated, and (e,f) after recovery.

Shape Memory Effect and Recovery of Optical Properties. The substantial polarization dependence of the stretched samples has already been discussed. The red- and blueshifts are more

prominent for the sample stretched with heating than for the sample stretched without heating, because the latter undergoes partial shape recovery when it is removed from the stretching jig. After heating under zero stress to drive shape recovery, both samples exhibit complete macroscopic shape recovery to their initial shape, but the polarized optical properties have a strong dependence on whether the samples had been stretched with or without heating. For the sample stretched without heating, the polarization dependence vanishes after shape recovery, implying the nanoscale arrangement of the Au NPs has also returned to its initial state.

For the sample heated during stretching, the red- and blueshifts in the polarized optical absorbance spectra after shape recovery are reduced but remain significant. Therefore, macroscopic shape recovery does not recover the nanoscale arrangement of the clusters of Au NP, which may be explained by irreversible flow of the soft component during combined heating and stretching. Even modest flow on the nanoscale could result in permanent effects from stretching that are preserved after macroscopic shape recovery. An important implication of this result is that changes in the microstructure of shape memory polymer nanocomposites during shape recovery can affect their properties and performance.

Optical Property Simulations. Simulations further support the interpretation of the of the polarized optical absorbance spectra and establish a relationship between the redshift in the SPR and the average interparticle spacing. As already established by optical absorbance spectroscopy, during stretching, the distance between Au NPs within clusters decreases along the length and increases perpendicular to the stretching direction, despite the Poisson effect. The resolution of high-resolution SEM is insufficient, however, to reliably quantify interparticle distances. We report simulations to support our interpretation of the polarized optical properties and to estimate the interparticle distances between the Au NPs whose plasmons are coupled.

Simulations are consistent with experiments and the above explanation, where stretching increases coupling of Au NPs along the parallel direction but decouples them in the perpendicular direction. Dimers of Au NPs were used for modelling for their simplicity and because many or the clusters are small. Dimers are a logical choice because this avoids having to otherwise choose an arbitrary number of particles in a cluster, and an arbitrary arrangement of the cluster, without experimental guidance. Furthermore, in many instances even for larger clusters of Au NPs, the shifts in the SPR plasmon peak are also likely dominated by pairwise interactions consistent with dimers.

The experimental and simulated optical absorbance spectra are compared chiefly based on the wavelength of the SPR maximum. Such comparison is limited in some instances by the width of the experimental SPR spectral peaks, as opposed to the narrow, simulated spectral peaks. For the three samples that exhibit polarization-dependent responses, interparticle separation distances can be chosen for the simulated dimers that produce polarized SPR maxima in good agreement with the those of the experiments, for both polarization directions simultaneously (Figure 5). The simulations of the dimer parallel (perpendicular) to its axis of interparticle separation are compared with the same direction in the experiments, along which the Au NPs are pulled closer together (further apart), which is redshifted (blueshifted) due to the strong (weak) plasmon coupling. The redshift for polarization parallel to the axis of interparticle separation is significantly stronger than the blueshift for polarization to the same axis. The interparticle separation distance, which is used as a parameter for matching the experimental and simulated results, is thus extracted from the analysis: For the sample with the largest red- and blue-shifts, stretched with heating, an interparticle separation distance of 3 nm is estimated. The sample stretched without heating and

the sample recovered after stretching with heating have similar red- and blue-shifts, and both match well with simulations for an interparticle separation distance of 5 nm.

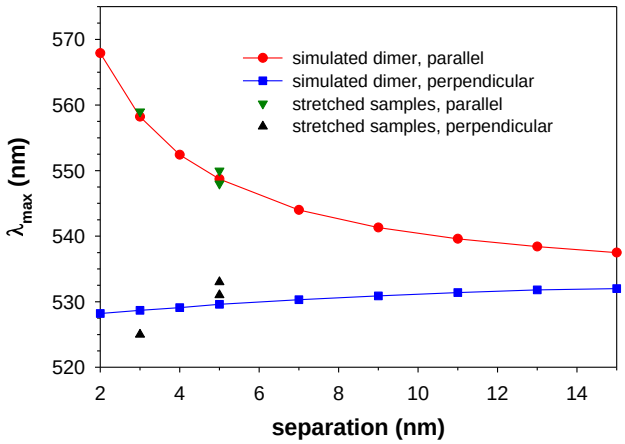

Figure 5.5: Maximum wavelength from optical absorbance spectra vs. interparticle surface-to-surface separation for dimers of Au NPs from simulations with data points for maximum wavelengths for three experimental samples added to match the simulations, thereby estimating the average interparticle distance. For simulations and experimental samples, parallel and perpendicular indicate the polarization direction with respect to the interparticle axis and the stretch direction, respectively.

As a further test of the method for comparing the maxima of experimental and simulated optical absorbance spectra to estimate the interparticle separation distance, we also compared the unpolarized spectra for the stretched samples (Supporting Information, Figure S8). The simulated unpolarized optical absorbance spectra can be obtained by averaging the extinction cross-sections of the parallel and perpendicular polarizations (Supporting Information, Figure S9). The unpolarized spectrum and the wavelength of its maximum are dominated by the parallel polarization direction. The interparticle separations already established from the polarized optical absorbance spectra for the three samples that exhibited polarization-dependent properties do not,

yield a good match with the unpolarized spectra (Supporting Information, Figure S8). This apparent lack of self-consistency can be attributed to the significantly greater breadth of the experimental peaks than the simulated peaks. Specifically, for short interparticle separation distances (≤ ~5 nm), averaging the extinction cross-sections of the parallel and perpendicular polarizations to obtain the unpolarized spectrum yields a redshifted spectrum with a significant shoulder to the blue (Supporting Information, Figure S9c). If the peaks for each polarization would be broader, as they are in the experimental spectrum, then the maximum wavelength of the unpolarized SPR peak would be blueshifted, since the effect of the peak for the perpendicular direction on the wavelength of the peak would be increased. Therefore, the shortcoming of comparing the unpolarized absorbance spectra at short wavelengths is the dependence on the widths of the peaks, which is mismatched between experiments and simulations. The Au NPs in the experimental samples have many different arrangements, with some having their SPRs more strongly coupled than others, which causes broadening in the optical absorbance spectrum. To highlight that the experimental peaks are much broader, the experimental and simulated polarized optical absorbance spectra for the three samples that exhibited significant polarization dependence are plotted Supporting Information, Figure S10.

Conclusions

In this work, formation of clusters of Au NPs during preparation of Diaplex nanocomposites causes strong coupling of their plasmons. This leads to significantly altered optical properties when these films are stretched, causing the average interparticle spacings to be shorter along the stretching direction and longer perpendicular to the stretching direction. Use of a SMP for the polymeric matrix allows setting a temporary shape with a significant polarization-

dependent optical response, followed by complete macroscale and nanoscale shape recovery if the film is not heated during stretching. In contrast, heating during stretching causes irreversible nanoscale changes within the clusters of Au NPs, while still allowing macroscale shape recovery. Simulations of the optical properties, based on a simple model of dimers of Au NPs, provide insights about the structural changes that occur during stretching and shape recovery.

These findings suggest future work could result in improved control over the optical property changes that occur during stretching and shape recovery. Specifically, use of advanced self-assembly techniques, potentially including microfabricated templates, could control the formation of clusters of NPs, which may be extended beyond Au. Simulations of both the mechanical response of the polymer and the optical response of the NP assembly would allow for the predictive design of responsive and reconfigurable plasmonic nanocomposites. The current materials and more advanced future materials could be applied as combined mechanical/thermal sensors or as materials with mechanically modulated optical properties.

Supporting Information. Details for optical property simulations, additional polarized and unpolarized experimental and simulated optical absorbance spectra, and analysis of unpolarized experimental and simulated optical absorbance spectra.

Supporting Information:

Details for Optical Property Simulations

Simulated optical extinction spectra of gold nanoparticles (GNPs) were computed as follows: First, the real and imaginary parts of the refractive index (RI) of Au was taken to be that suggested in Section 3.6 of Ref. [183]. To simplify calculations, a representative GNP diameter, d_{avg}, was chosen to approximate the extinction cross-section, C_{ext}, over the experimentally observed size distribution of GNPs, (15.6 ± 2.8 nm), as follows. Bohren-Huffman Mie scattering computations[184] were performed for wavelengths spanning λ = 500-600 nm of isolated Au nanospheres in tetrahydrofuran (THF). A RI for THF of 1.4060 was chosen, which is within a range of commonly reported values. To simulate the extinction spectra of the GNPs over their size distribution, $C_{ext}(\lambda)$ was computed for each GNP diameter measured from a transmission electron micrograph of 200 GNPs, then averaged. A resulting peak wavelength of λ_{peak} = 520.40 nm was obtained. Then, $C_{ext}(\lambda)$ of single GNPs of varying diameter were simulated to match λ_{peak} with that of the distribution, resulting in d_{avg} = 17.0 nm. The fact that d_{avg} is larger than the mean of the GNP size distribution is expected due to the nonlinear scaling of light scattering with particle size. The simulated extinction spectrum using a single representative d_{avg} closely matches the experimental extinction spectrum obtained from the GNPs in THF (see Figure S1), with the experimental λ_{peak} = 522 nm.

To simulate the optical coupling of GNPs in polymer matrices, we chose the *T*-matrix method because it is exact up to the order of the expansion computed, and has been extensively validated experimentally.[185] A *T*-matrix program appropriate for computing light scattering from ensembles of spheres[186] was downloaded from http://www.giss.nasa.gov/~crmim/t_matrix.html, compiled, and called by a custom Matlab script. The program was validated against a published

scattering matrix table for a bisphere (two identical, touching spheres) tilted at 50 degrees,[187] where we found an average difference between our method and this reference of 0.64%. To simulate GNPs in Diaplex, we chose the Diaplex RI = 1.5823 (measured at 589 nm).[188] Finally, the program was used to compute $C_{ext}(\lambda)$ for gold bispheres of diameter d_{avg} as a function of separation distances between 1-15 nm. Bispheres were displaced along a transverse (x) axis relative to the light propagation (z) axis, and $C_{ext}(\lambda)$ was computed for input light polarized either parallel (x), perpendicular (y), or unpolarized (as an average of parallel and perpendicular C_{ext}). Then, λ_{peak} was determined within a step size of 0.1 nm in the range λ = 500-650 nm for each spectrum.

Photograph of Jig for Stretching Composite Films

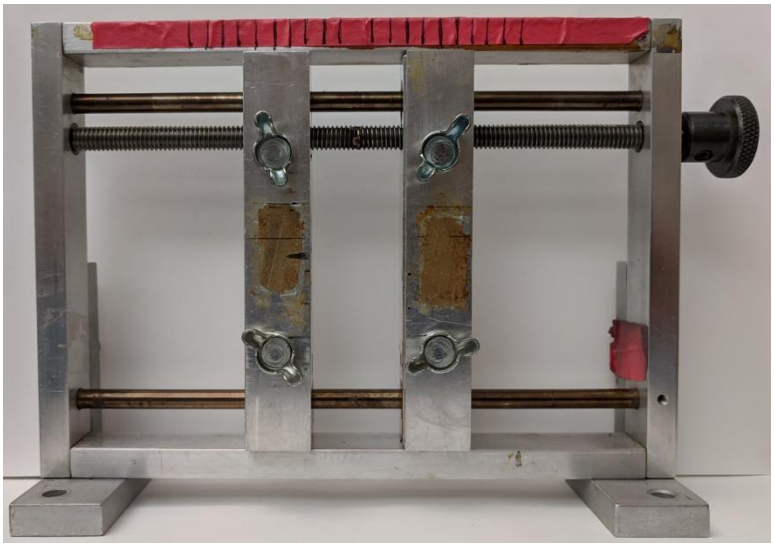

Figure S1: Photograph of Jig for Stretching Composite Films.

Additional Experimental Optical Absorbance Spectra

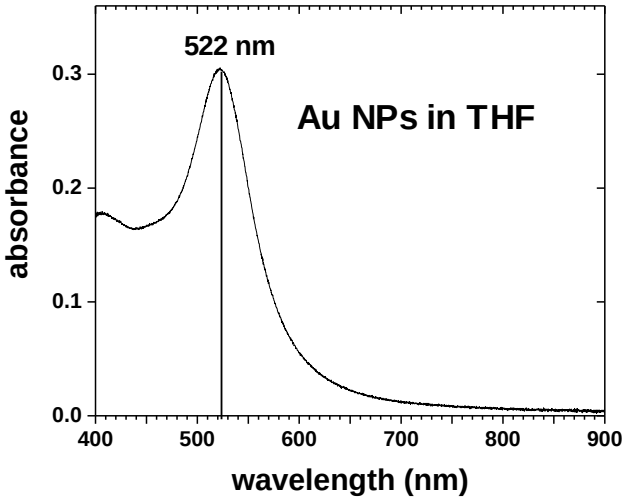

Figure S2: Unpolarized optical absorbance spectrum of Au NPs dispersed in THF.

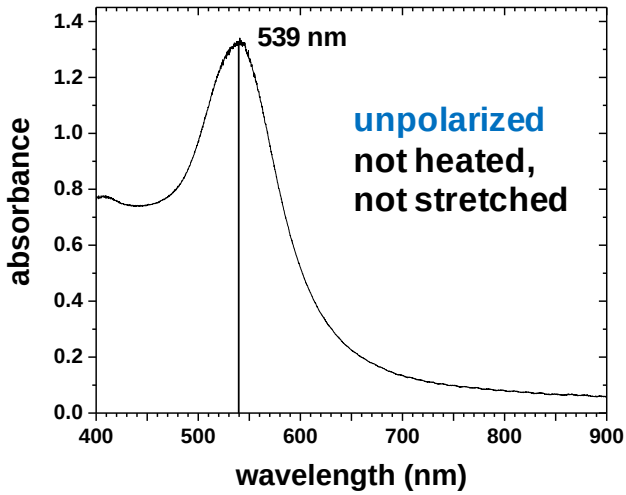

Figure S3: Unpolarized optical absorbance spectrum of Au NPs in a Diaplex film before stretching or heating.

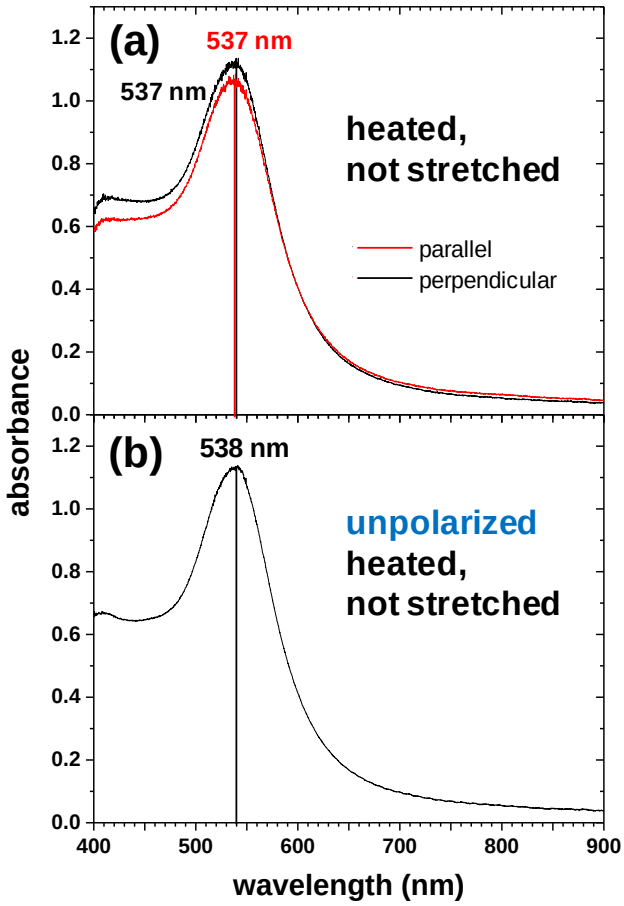

Figure S4: (a) Polarized and (b) unpolarized optical absorbance spectrum of Au NPs in a Diaplex film after heating without stretching.

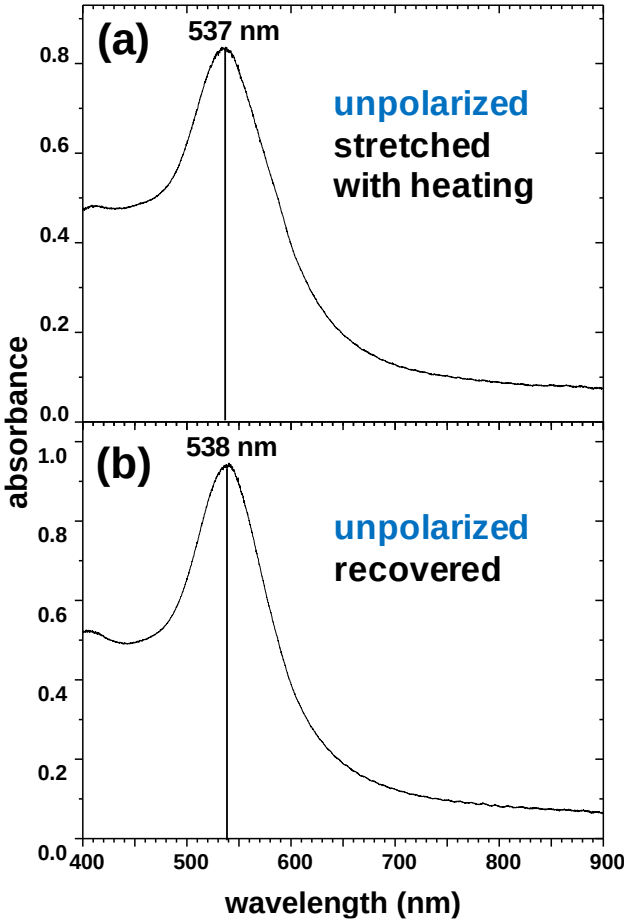

Figure S5: (a) Unpolarized optical absorbance spectrum of Au NPs in a Diaplex film (a) after stretching with heating and (b) after (a) and heating under zero stress to drive shape recovery.

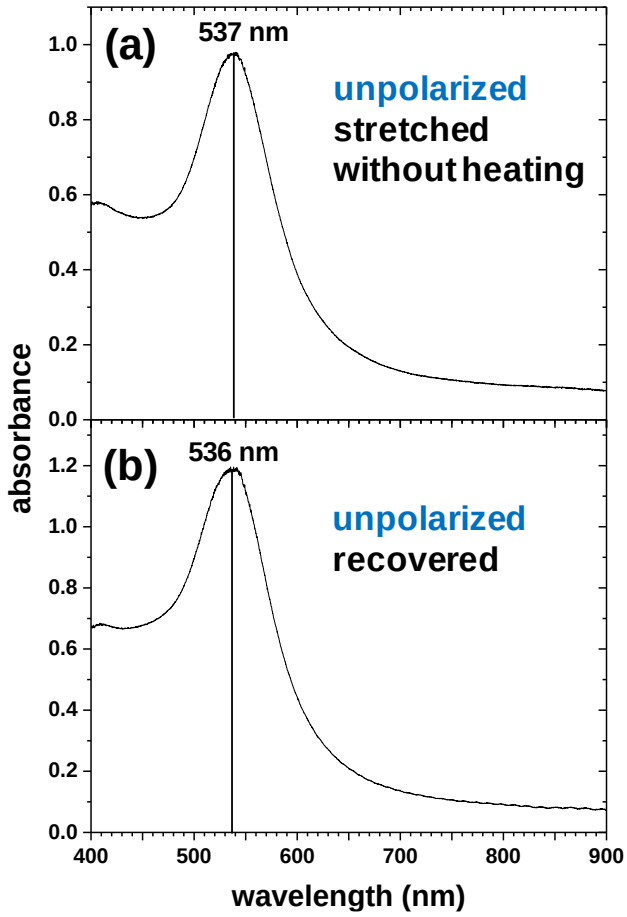

Figure S6: (a) Unpolarized optical absorbance spectrum of Au NPs in a Diaplex film (a) after stretching without heating and (b) after (a) and heating under zero stress to drive shape recovery.

Simulations of Optical Properties

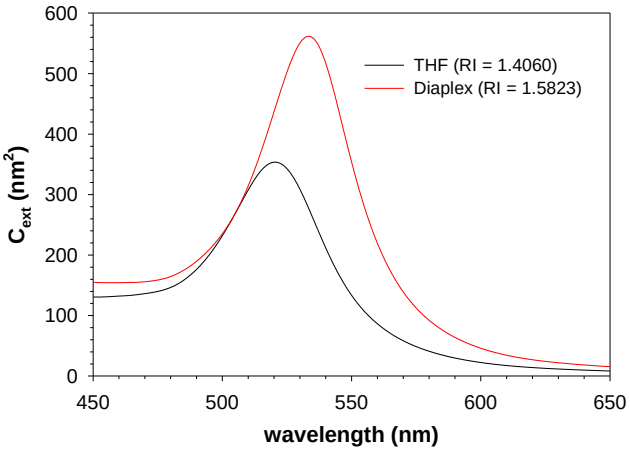

Figure S7: Simulations of the effect of refractive index (RI) of the environment on the extinction cross section for isolated, decoupled Au NPs in THF (maximum extinction at 520 nm) and in Diaplex (maximum extinction at 533 nm).

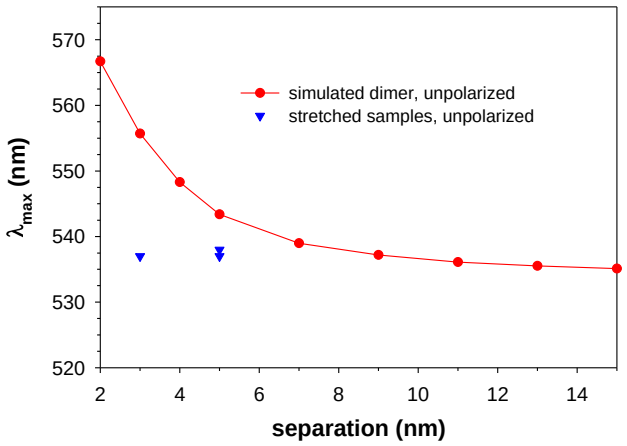

Figure S8: Maximum wavelength from unpolarized optical absorbance spectra vs. interparticle surface-to-surface separation for dimers of Au NPs from simulations with data points for maximum wavelengths for three experimental samples added with separation distances established from the polarized optical absorbance spectra (see Figure 5).

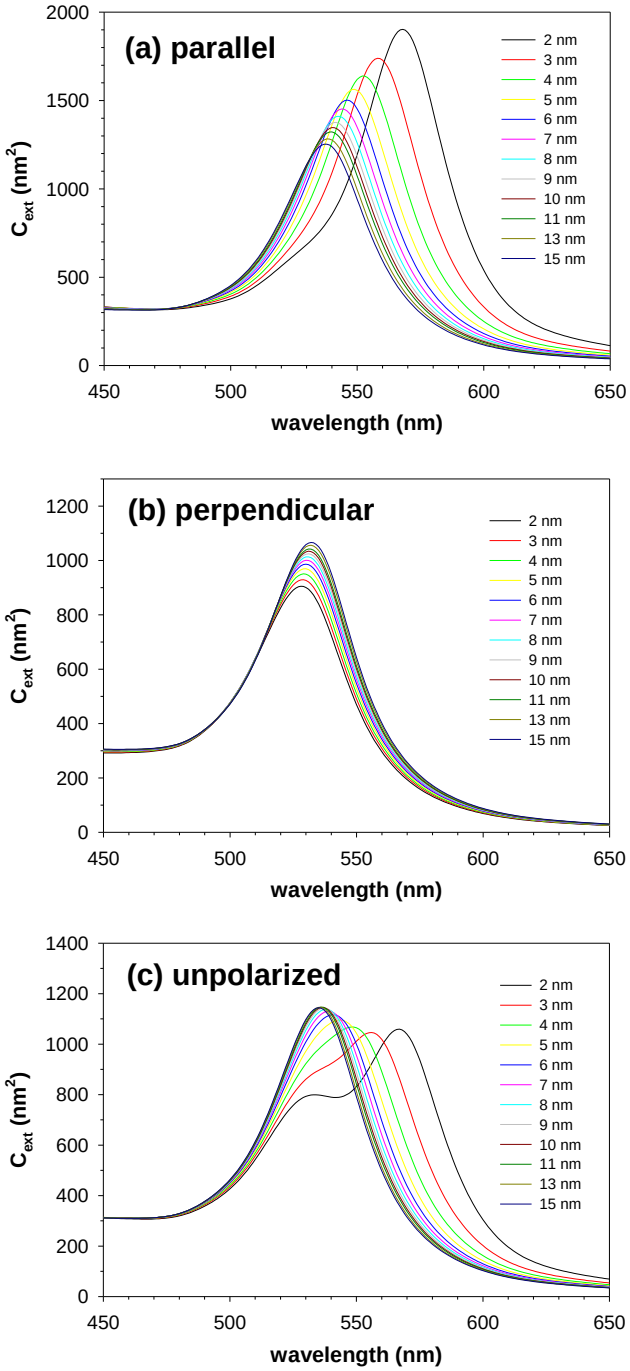

Figure S9: Simulations of the extinction cross section for dimers of Au NPs of with different surface-to-surface separation distances when illuminated with light polarized (a) parallel or (b) perpendicular to the axis connecting the centers of the NPs, or (c) unpolarized light.

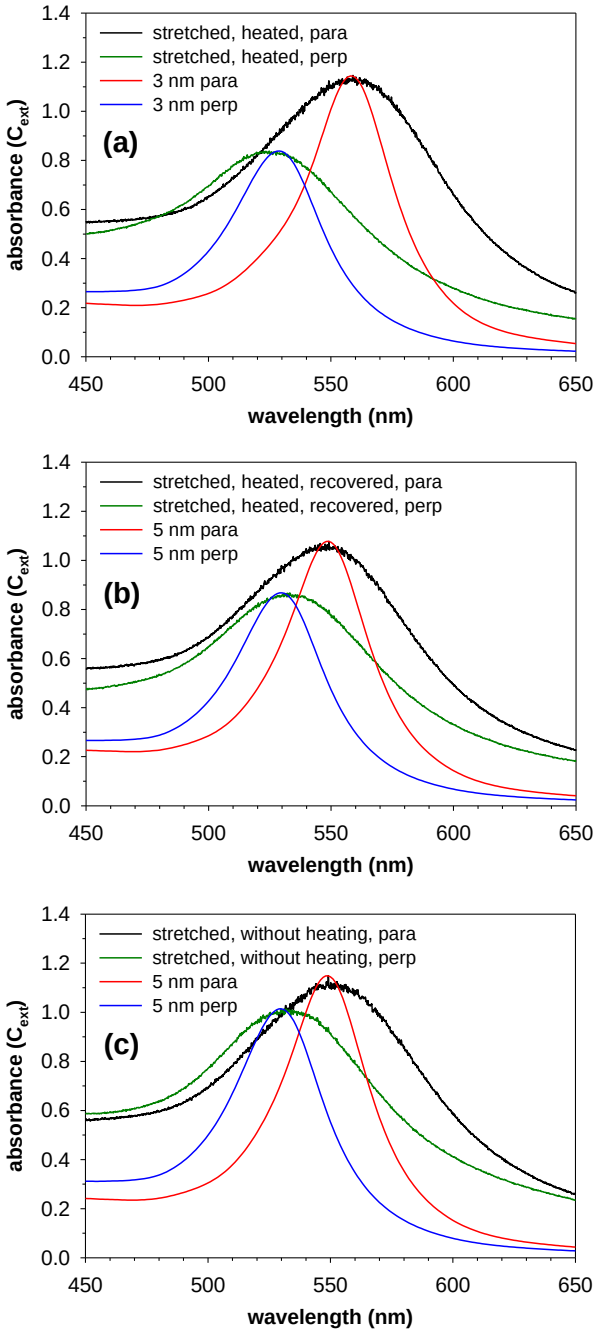

Figure S10: Experimental optical absorbance spectra for three samples exhibiting prominent polarization-dependent optical properties with overlaid, normalized simulations of the extinction cross-sections for dimers of Au NPs at distances selected to match the experimental spectra: (a) stretched with heating (see Figure 2a) and (b) then recovered (see Figure 2b), and (c) stretched without heating (see Figure 3a).

Chapter 6: Conclusion and Outlook

6.1 Summary

Integration of plasmonic NPs with SMPs offers control of the macroscopic shape of composite films with actuation driven by heat or light. In this study, the response was observed by means of optical absorbance spectroscopy and SEM images showing clustering of NPs in mechanically strained films. Plasmon coupling of NPs in polymers gives rise to polarization of light. These effects were partially irreversible when the films were heated while stretching, which results from a local change in the morphology of the SMP.

6.2 Future Work

Self-assembly of NPs within polymers is a rich system for investigating and engineering the physical properties of polymer composites. Composites with advanced mechanical and thermal properties could be prepared following methods studied in this work. The sensitivity of the SME to the heating conditions during stretching is potentially useful for thermal history sensors, and the plasmon ruler concept could also be applied more broadly for understanding the behaviors of assemblies of plasmonic NPs integrated within or on top of stimulus-responsive polymers.

REFERENCES

1. Malhotra, B. D.; Ali, M. A., Chapter 1 - Nanomaterials in biosensors: fundamentals and applications. In *Nanomaterials for Biosensors*, Malhotra, B. D.; Ali, M. A., Eds. William Andrew Publishing: 2018; pp 1-74.
2. Reibold, M.; Pätzke, N.; Levin, A. A.; Kochmann, W.; Shakhverdova, I. P.; Paufler, P.; Meyer, D. C., Structure of several historic blades at nanoscale. *Cryst. Res. Technol.* **2009,** *44* (10), 1139-1146.
3. Polette-Niewold, L. A.; Manciu, F. S.; Torres, B.; Alvarado, M., Jr.; Chianelli, R. R., Organic/inorganic complex pigments: ancient colors Maya Blue. *J. Inorg. Biochem.* **2007,** *101* (11-12), 1958-73.
4. Freestone, I.; Meeks, N.; Sax, M.; Higgitt, C., The Lycurgus cup — a Roman nanotechnology. *Gold Bulletin* **2007,** *40* (4), 270-277.
5. Schaming, D.; Remita, H., Nanotechnology: from the ancient time to nowadays. *Foundations of Chemistry* **2015,** *17* (3), 187-205.
6. Ho, A. Y. Y.; Yeo, L. P.; Lam, Y. C.; Rodríguez, I., Fabrication and analysis of gecko-inspired hierarchical polymer nanosetae. *ACS Nano* **2011,** *5* (3), 1897-1906.
7. Dai, B.; Wang, J.; Xiong, Z.; Zhan, X.; Dai, W.; Li, C.-C.; Feng, S.-P.; Tang, J., Programmable artificial phototactic microswimmer. *Nat. Nanotechnol.* **2016,** *11*, 1087-1092
8. Ali, J.; Cheang, U. K.; Martindale, J. D.; Jabbarzadeh, M.; Fu, H. C.; Jun Kim, M., Bacteria-inspired nanorobots with flagellar polymorphic transformations and bundling. *Scientific Reports* **2017,** *7* (1), 14098.

9. Narasimhan, V.; Siddique, R. H.; Lee, J. O.; Kumar, S.; Ndjamen, B.; Du, J.; Hong, N.; Sretavan, D.; Choo, H., Multifunctional biophotonic nanostructures inspired by the longtail glasswing butterfly for medical devices. *Nat. Nanotechnol.* **2018,** *13* (6), 512-519.

10. Papadopoulos, C., Nanofabrication : principles and applications. **2016**.

11. Steed, J. W.; Atwood, J. L., *Supramolecular chemistry*. Wiley: Chichester, 2012.

12. Jain, S.; Hirst, D. G.; O'Sullivan, J. M., Gold nanoparticles as novel agents for cancer therapy. *The British Journal of Radiology* **2012,** *85* (1010), 101-113.

13. Sundar, S.; Prajapati, V. K., Drug targeting to infectious diseases by nanoparticles surface functionalized with special biomolecules. *Curr. Med. Chem.* **2012,** *19* (19), 3196-3202.

14. Estelrich, J.; Sánchez-Martín, M. J.; Busquets, M. A., Nanoparticles in magnetic resonance imaging: from simple to dual contrast agents. *International Journal of Nanomedicine* **2015,** *10*, 1727-1741.

15. Edwards, P. P.; Thomas, J. M., Gold in a metallic divided state--from Faraday to present-day nanoscience. *Angew. Chem.* **2007,** *46* (29), 5480-5486.

16. Turkevich, J.; Stevenson, P. C.; Hillier, J., A study of the nucleation and growth processes in the synthesis of colloidal gold. *Discussions of the Faraday Society* **1951,** *11* (0), 55-75.

17. Frens, G., Controlled nucleation for the regulation of the particle size in monodisperse gold suspensions. *Nature Physical Science* **1973,** *241*, 20-22.

18. Kimling, J.; Maier, M.; Okenve, B.; Kotaidis, V.; Ballot, H.; Plech, A., Turkevich method for gold nanoparticle synthesis revisited. *The Journal of Physical Chemistry B* **2006,** *110* (32), 15700-15707.

19. Polte, J., Fundamental growth principles of colloidal metal nanoparticles – a new perspective. *CrystEngComm* **2015,** *17* (36), 6809-6830.

20. Optical properties of gold colloids formed in inverse micelles. *The Journal of Chemical Physics* **1993,** *98* (12), 9933-9950.

21. Brust, M.; Walker, M.; Bethell, D.; Schiffrin, D. J.; Whyman, R., Synthesis of thiol-derivatised gold nanoparticles in a two-phase Liquid–Liquid system. *J. Chem. Soc., Chem. Commun.* **1994,** (7), 801-802.

22. Hiramatsu, H.; Osterloh, F. E., A simple large-scale synthesis of nearly monodisperse gold and silver nanoparticles with adjustable sizes and with exchangeable surfactants. *Chem. Mater.* **2004,** *16* (13), 2509-2511.

23. Gomez, S.; Philippot, K.; Collière, V.; Chaudret, B.; Senocq, F.; Lecante, P., Gold nanoparticles from self-assembled gold() amine precursors. *Chem. Commun.* **2000,** (19), 1945-1946.

24. Laguna, A., *Modern supramolecular gold chemistry : gold-metal interactions and applications*. Wiley-VCH ; John Wiley [distributor]: Weinheim; Chichester, 2008.

25. Sardar, R.; Funston, A. M.; Mulvaney, P.; Murray, R. W., Gold nanoparticles: past, present, and future. *Langmuir* **2009,** *25* (24), 13840-13851.

26. Thakor, A. S.; Jokerst, J.; Zavaleta, C.; Massoud, T. F.; Gambhir, S. S., Gold nanoparticles: a revival in precious metal administration to patients. *Nano Lett.* **2011,** *11* (10), 4029-4036.

27. Colours in metal glasses, in metallic films and in metallic solutions.—II. *Proceedings of the Royal Society of London. Series A* **1905,** *76* (511), 370-373.

28. Colloidal metal in aluminum-oxide. *J. Appl. Phys.* **1978,** *49* (5), 2929-2934.

29. Rai, P. D. M.; Shegokar, P. D. R., *Metal nanoparticles in pharma*. 2017.

30. Snow, A. W.; Wohltjen, H., Size-induced metal to semiconductor transition in a stabilized gold cluster ensemble. *Chem. Mater.* **1998,** *10* (4), 947-949.

31. Suh, J. Y.; Donev, E. U.; Ferrara, D. W.; Tetz, K. A.; Feldman, L. C.; R. F. Haglund, J., Modulation of the gold particle–plasmon resonance by the metal–semiconductor transition of vanadium dioxide. *Journal of Optics A: Pure and Applied Optics* **2008,** *10* (5), 055202.

32. Mulvaney, P., Surface plasmon spectroscopy of nanosized metal particles. *Langmuir* **1996,** *12* (3), 788-800.

33. Talley, C. E.; Jackson, J. B.; Oubre, C.; Grady, N. K.; Hollars, C. W.; Lane, S. M.; Huser, T. R.; Nordlander, P.; Halas, N. J., Surface-enhanced Raman scattering from individual Au nanoparticles and nanoparticle dimer substrates. *Nano Lett.* **2005,** *5* (8), 1569-1574.

34. Baida, H.; Christofilos, D.; Maioli, P.; Crut, A.; Del Fatti, N.; Vallée, F., Surface plasmon resonance spectroscopy of single surfactant-stabilized gold nanoparticles. *The European Physical Journal D* **2011,** *63* (2), 293-299.

35. Tian, F.; Bonnier, F.; Casey, A.; Shanahan, A. E.; Byrne, H. J., Surface enhanced Raman scattering with gold nanoparticles: effect of particle shape. *Analytical Methods* **2014,** *6* (22), 9116-9123.

36. Bond, G. C., The catalytic properties of gold. *Gold Bulletin* **1972,** *5* (1), 11-13.

37. Torres Sanchez, R. M.; Ueda, A.; Tanaka, K.; Haruta, M., Selective oxidation of CO in hydrogen over gold supported on manganese oxides. *J. Catal.* **1997,** *168* (1), 125-127.

38. Haruta, M., Size- and support-dependency in the catalysis of gold. *Catal. Today* **1997,** *36* (1), 153-166.

39. Murawsk, M.; Skrzypczak, A.; Kozak, M. In *Structure and morphology of gold nanoparticles in solution studied by TEM, SAXS and UV-Vis*, 2012/04//; Instytut Fizyki, Polska Akademia Nauk: pp 888-892.

40. Buhr, E.; Senftleben, N.; Klein, T.; Bergmann, D.; Gnieser, D.; Frase, C. G.; Bosse, H., Characterization of nanoparticles by scanning electron microscopy in transmission mode. *Meas. Sci. Technol.* **2009,** *20* (8), 084025.

41. Sobczak-Kupiec, A.; Malina, D.; Zimowska, M.; Wzorek, Z., Characterization of gold nanoparticles for various medical application. *Digest Journal of Nanomaterials & Biostructures (DJNB)* **2011,** *6* (2), 803-808.

42. Maier, S. A., *Plasmonics : fundamentals and applications*. 2015.

43. Kelly, K. L.; Coronado, E.; Zhao, L. L.; Schatz, G. C., The optical properties of metal nanoparticles: the influence of size, shape, and dielectric environment. *The Journal of Physical Chemistry B* **2003,** *107* (3), 668-677.

44. Garcia, M. A., Surface plasmons in metallic nanoparticles: fundamentals and applications. *J. Phys. D: Appl. Phys.* **2011,** *44* (28), 283001.

45. Nguyen, H. H.; Park, J.; Kang, S.; Kim, M., Surface plasmon resonance: a versatile technique for biosensor applications. *Sensors* **2015,** *15* (5), 10481-10510.

46. Link, S.; El-Sayed, M. A., Spectral properties and relaxation dynamics of surface plasmon electronic oscillations in gold and silver nanodots and nanorods. *The Journal of Physical Chemistry B* **1999,** *103* (40), 8410-8426.

47. Dahmen, C.; Schmidt, B.; von Plessen, G., Radiation damping in metal nanoparticle pairs. *Nano Lett.* **2007,** *7* (2), 318-322.

48. Englebienne, P.; Hoonacker, A. V.; Verhas, M., Surface plasmon resonance: principles, methods and applications in biomedical sciences. *Spectroscopy* **2003,** *17* (2,3), 255-273.

49. Willets, K. A.; Van Duyne, R. P., Localized surface plasmon resonance spectroscopy and sensing. *Annu. Rev. Phys. Chem.* **2007,** *58* (1), 267-297.

50. Austin, L. A.; Kang, B.; El-Sayed, M. A., Probing molecular cell event dynamics at the single-cell level with targeted plasmonic gold nanoparticles: A review. *Nano Today* **2015,** *10* (5), 542-558.

51. Noguez, C., Surface plasmons on metal nanoparticles: the influence of shape and physical environment. *The Journal of Physical Chemistry C* **2007,** *111* (10), 3806-3819.

52. Petryayeva, E.; Krull, U. J., Localized surface plasmon resonance: Nanostructures, bioassays and biosensing—A review. *Anal. Chim. Acta* **2011,** *706* (1), 8-24.

53. Amendola, V.; Pilot, R.; Frasconi, M.; Maragò, O. M.; Iatì, M. A., Surface plasmon resonance in gold nanoparticles: a review. *J. Phys.: Condens. Matter* **2017,** *29* (20), 203002.

54. Jain, P. K.; Lee, K. S.; El-Sayed, I. H.; El-Sayed, M. A., Calculated absorption and scattering properties of gold nanoparticles of different size, shape, and composition: Applications in biological imaging and biomedicine. *The Journal of Physical Chemistry B* **2006,** *110* (14), 7238-7248.

55. Lu, X.; Rycenga, M.; Skrabalak, S. E.; Wiley, B.; Xia, Y., Chemical synthesis of novel plasmonic nanoparticles. *Annu. Rev. Phys. Chem.* **2009,** *60* (1), 167-192.

56. Mayer, K. M.; Hafner, J. H., Localized surface plasmon resonance sensors. *Chem. Rev.* **2011,** *111* (6), 3828-3857.

57. Amendola, V.; Rizzi, G. A.; Polizzi, S.; Meneghetti, M., Synthesis of gold nanoparticles by laser ablation in toluene: quenching and recovery of the surface plasmon absorption. *The Journal of Physical Chemistry B* **2005,** *109* (49), 23125-23128.

58. Tan, C. L.; Jang, S. J.; Lee, Y. T., Localized surface plasmon resonance with broadband ultralow reflectivity from metal nanoparticles on glass and silicon subwavelength structures. *Opt. Express* **2012,** *20* (16), 17448-17455.

59. Amendola, V., Surface plasmon resonance of silver and gold nanoparticles in the proximity of graphene studied using the discrete dipole approximation method. *Phys. Chem. Chem. Phys.* **2016,** *18* (3), 2230-2241.

60. Zhao, Y.; Li, S.; Zeng, Y.; Jiang, Y., Synthesis and properties of Ag/ZnO core/shell nanostructures prepared by excimer laser ablation in liquid. *APL Materials* **2015,** *3* (8), 086103.

61. Kadkhodazadeh, S.; de Lasson, J. R.; Beleggia, M.; Kneipp, H.; Wagner, J. B.; Kneipp, K., Scaling of the surface plasmon resonance in gold and silver dimers probed by EELS. *The Journal of Physical Chemistry C* **2014,** *118* (10), 5478-5485.

62. Wang, L.-D.; Zhang, T.; Zhang, X.-Y.; Song, Y.-J.; Li, R.-Z.; Zhu, S.-Q., Optical properties of Ag nanoparticle-polymer composite film based on two-dimensional Au nanoparticle array film. *Nanoscale Res. Lett.* **2014,** *9* (1), 155.

63. Negre, C. F. A.; Sánchez, C. G., Effect of molecular adsorbates on the plasmon resonance of metallic nanoparticles. *Chem. Phys. Lett.* **2010,** *494* (4), 255-259.

64. Rander, T.; Staiger, M.; Richter, R.; Zimmermann, T.; Landt, L.; Wolter, D.; Dahl, J. E.; Carlson, R. M. K.; Tkachenko, B. A.; Fokina, N. A.; Schreiner, P. R.; Möller, T.; Bostedt, C., Electronic structure tuning of diamondoids through functionalization. *The Journal of Chemical Physics* **2013,** *138* (2), 024310.

65. Malola, S.; Lehtovaara, L.; Enkovaara, J.; Häkkinen, H., Birth of the localized surface plasmon resonance in monolayer-protected gold nanoclusters. *ACS Nano* **2013,** *7* (11), 10263-10270.

66. Foerster, B.; Spata, V. A.; Carter, E. A.; Sönnichsen, C.; Link, S., Plasmon damping depends on the chemical nature of the nanoparticle interface. *Science Advances* **2019,** *5* (3), eaav0704.

67. Špringer, T.; Ermini, M. L.; Špačková, B.; Jabloňků, J.; Homola, J., Enhancing sensitivity of surface plasmon resonance biosensors by functionalized gold nanoparticles: Size matters. *Anal. Chem.* **2014,** *86* (20), 10350-10356.

68. Dykman, L. A.; Khlebtsov, N. G., Gold nanoparticles in biology and medicine: recent advances and prospects. *Acta naturae* **2011,** *3* (2), 34-55.

69. Shukla, R.; Bansal, V.; Chaudhary, M.; Basu, A.; Bhonde, R. R.; Sastry, M., Biocompatibility of gold nanoparticles and their endocytotic fate inside the cellular compartment: A microscopic overview. *Langmuir* **2005,** *21* (23), 10644-10654.

70. Hill, R. T.; Mock, J. J.; Hucknall, A.; Wolter, S. D.; Jokerst, N. M.; Smith, D. R.; Chilkoti, A., Plasmon ruler with angstrom length resolution. *ACS Nano* **2012,** *6* (10), 9237-9246.

71. Jain, P. K.; El-Sayed, M. A., Plasmonic coupling in noble metal nanostructures. *Chem. Phys. Lett.* **2010,** *487* (4), 153-164.

72. Halas, N. J.; Lal, S.; Chang, W.-S.; Link, S.; Nordlander, P., Plasmons in strongly coupled metallic nanostructures. *Chem. Rev.* **2011,** *111* (6), 3913-3961.

73. Lange, H.; Juárez, B. H.; Carl, A.; Richter, M.; Bastús, N. G.; Weller, H.; Thomsen, C.; von Klitzing, R.; Knorr, A., Tunable plasmon coupling in distance-controlled gold nanoparticles. *Langmuir* **2012,** *28* (24), 8862-8866.

74. Wang, X.; Gogol, P.; Cambril, E.; Palpant, B., Near- and far-field effects on the plasmon coupling in gold nanoparticle arrays. *The Journal of Physical Chemistry C* **2012,** *116* (46), 24741-24747.

75. Reinhard, B. M.; Siu, M.; Agarwal, H.; Alivisatos, A. P.; Liphardt, J., Calibration of dynamic molecular rulers based on plasmon coupling between gold nanoparticles. *Nano Lett.* **2005,** *5* (11), 2246-2252.

76. Atwood, J. L.; Steed, J. W., Supramolecular chemistry. **2013**.

77. Dahman, Y., *Nanotechnology and functional materials for engineers*. 2017.

78. Grzelczak, M.; Liz-Marzán, L. M.; Klajn, R., Stimuli-responsive self-assembly of nanoparticles. *Chem. Soc. Rev.* **2019,** *48* (5), 1342-1361.

79. Zhang, J. Z.; Wang, Z. L.; Liu, J.; Chen, S.; Liu, G.-y., Self-assembled nanostructures. **2004**.

80. Guo, Z.; Tan, L., *Fundamentals and applications of nanomaterials*. Artech House: Boston, 2009.

81. Xu, J.-F.; Niu, L.-Y.; Chen, Y.-Z.; Wu, L.-Z.; Tung, C.-H.; Yang, Q.-Z., Hydrogen bonding directed self-assembly of small-molecule amphiphiles in water. *Org. Lett.* **2014,** *16* (15), 4016-4019.

82. Hamelin, B.; Jullien, L.; Derouet, C.; Hervé du Penhoat, C.; Berthault, P., Self-assembly of a molecular capsule driven by electrostatic interaction in aqueous solution. *J. Am. Chem. Soc.* **1998,** *120* (33), 8438-8447.

83. Choi, I. S.; Bowden, N.; Whitesides, G. M., Shape-selective recognition and self-assembly of mm-scale components. *J. Am. Chem. Soc.* **1999,** *121* (8), 1754-1755.

84. Sánchez-Iglesias, A.; Grzelczak, M.; Altantzis, T.; Goris, B.; Pérez-Juste, J.; Bals, S.; Van Tendeloo, G.; Donaldson, S. H.; Chmelka, B. F.; Israelachvili, J. N.; Liz-Marzán, L. M., Hydrophobic interactions modulate self-assembly of nanoparticles. *ACS Nano* **2012,** *6* (12), 11059-11065.

85. DNA self-assembly scaled up. *Nature* **2017,** *552* (7684).

86. Whitesides, G. M.; Boncheva, M., Beyond molecules: self-assembly of mesoscopic and macroscopic components. *Proceedings of the National Academy of Sciences* **2002,** *99* (8), 4769.

87. Piguet, C.; Borkovec, M.; Hamacek, J.; Zeckert, K., Strict self-assembly of polymetallic helicates: the concepts behind the semantics. *Coord. Chem. Rev.* **2005,** *249* (5), 705-726.

88. Veerman, C.; de Schiffart, G.; Sagis, L. M. C.; van der Linden, E., Irreversible self-assembly of ovalbumin into fibrils and the resulting network rheology. *Int. J. Biol. Macromol.* **2003,** *33* (1), 121-127.

89. Albert, A. P., Gating mechanisms of canonical transient receptor potential channel proteins: role of phosphoinositols and diacylglycerol. In *Transient Receptor Potential Channels*, Islam, M. S., Ed. Springer Netherlands: Dordrecht, 2011; pp 391-411.

90. Kuehl, C. J.; Huang, S. D.; Stang, P. J., Self-assembly with postmodification: kinetically stabilized metalla-supramolecular rectangles. *J. Am. Chem. Soc.* **2001,** *123* (39), 9634-9641.

91. Ellis, R. J., Assembly chaperones: a perspective. *Philosophical transactions of the Royal Society of London. Series B, Biological sciences 368* (1617), 20110398-20110398.

92. Kim, B. H.; Kim, J. Y.; Kim, S. O., Directed self-assembly of block copolymers for universal nanopatterning. *Soft Matter* **2013,** *9* (10), 2780-2786.

93. Yin, Y.; Lu, Y.; Gates, B.; Xia, Y., Template-assisted self-assembly: a practical route to complex aggregates of monodispersed colloids with well-defined sizes, shapes, and structures. *J. Am. Chem. Soc.* **2001,** *123* (36), 8718-8729.

94. Zhu, Y.; Liu, W.; Zhang, X.; He, J.; Chen, J.; Wang, Y.; Cao, T., Directing silicon–graphene self-assembly as a core/shell anode for high-performance lithium-ion batteries. *Langmuir* **2013,** *29* (2), 744-749.

95. Bhattacharya, M., Polymer nanocomposites-a comparison between carbon nanotubes, graphene, and clay as nanofillers. *Materials (Basel, Switzerland)* **2016,** *9* (4), 262.

96. Chu, J.; Young, R. J.; Slater, T. J. A.; Burnett, T. L.; Coburn, B.; Chichignoud, L.; Vuilleumier, A.; Li, Z., Realizing the theoretical stiffness of graphene in composites through confinement between carbon fibers. *Composites Part A: Applied Science and Manufacturing* **2018,** *113*, 311-317.

97. Lin, Y.-C.; Chen, C.-Y.; Chen, H.-L.; Hashimoto, T.; Chen, S.-A.; Li, Y.-C., Hierarchical self-assembly of nanoparticles in polymer matrix and the nature of the interparticle interaction. *The Journal of Chemical Physics* **2015,** *142* (21), 214905.

98. Genix, A.-C.; Oberdisse, J., Nanoparticle self-assembly: from interactions in suspension to polymer nanocomposites. *Soft Matter* **2018,** *14* (25), 5161-5179.

99. Chen, Y.; Wang, Z.; He, Y.; Yoon, Y. J.; Jung, J.; Zhang, G.; Lin, Z., Light-enabled reversible self-assembly and tunable optical properties of stable hairy nanoparticles. *Proceedings of the National Academy of Sciences* **2018,** *115* (7), E1391.

100. Huebner, D.; Rossner, C.; Vana, P., Light-induced self-assembly of gold nanoparticles with a photoresponsive polymer shell. *Polymer* **2016,** *107*, 503-508.

101. Kanehara, M.; Kodzuka, E.; Teranishi, T., Self-assembly of small gold nanoparticles through interligand interaction. *J. Am. Chem. Soc.* **2006,** *128* (40), 13084-13094.

102. Lendlein, A.; Kelch, S., Shape-memory polymers. *Angewandte Chemie International Edition* **2002,** *41* (12), 2034-2057.

103. Imran Khan, M.; Zagho, M. M.; Shakoor, R. A., A brief overview of shape memory effect in thermoplastic polymers. In *Smart polymer nanocomposites: energy harvesting, self-healing and shape memory applications*, Ponnamma, D.; Sadasivuni, K. K.; Cabibihan, J.-J.; Al-Maadeed, M. A.-A., Eds. Springer International Publishing: Cham, 2017; pp 281-301.

104. Dávid, K.; Gábor, B.; Zsolt, D.; Pál, H., Study of shape memory alloys and the phase transition by DMTA and DSC measurements. *Journal of Physics: Conference Series* **2015,** *602*, 012024.

105. Liu, C.; Qin, H.; Mather, P. T., Review of progress in shape-memory polymers. *J. Mater. Chem.* **2007,** *17* (16), 1543-1558.

106. Patil, D.; Song, G., A review of shape memory material's applications in the offshore oil and gas industry. *Smart Materials and Structures* **2017,** *26* (9), 093002.

107. Thomas, S.; Yang, W., *Advances in polymer processing: From macro- to nano- scales*. Elsevier Science: 2009.

108. Mishra, S. R. Selective Actuation of Polymer Nanocomposites by Controlling Properties of Magnetic and Plasmonic Nanoparticles for Soft Robotics Applications. North Carolina State University, Raleigh, NC, 2016.

109. Pretsch, T., Review on the functional determinants and durability of shape memory polymers. *Polymers* **2010,** *2* (3).

110. Meng, H.; Li, G., A review of stimuli-responsive shape memory polymer composites. *Polymer* **2013,** *54* (9), 2199-2221.

111. Safranski, D. L., Chapter One - Introduction to shape-memory polymers. In *Shape-Memory Polymer Device Design*, Safranski, D. L.; Griffis, J. C., Eds. William Andrew Publishing: 2017; pp 1-22.

112. Habault, D.; Zhang, H.; Zhao, Y., Light-triggered self-healing and shape-memory polymers. *Chem. Soc. Rev.* **2013,** *42* (17), 7244-7256.

113. Mohr, R.; Kratz, K.; Weigel, T.; Lucka-Gabor, M.; Moneke, M.; Lendlein, A., Initiation of shape-memory effect by inductive heating of magnetic nanoparticles in thermoplastic polymers. *Proc. Natl. Acad. Sci. U. S. A.* **2006,** *103* (10), 3540-3545.

114. Naskar, A. K.; Keum, J. K.; Boeman, R. G., Polymer matrix nanocomposites for automotive structural components. *Nat. Nanotechnol.* **2016,** *11*, 1026-1030.

115. Balazs, A. C.; Emrick, T.; Russell, T. P., Nanoparticle polymer composites: Where two small worlds meet. *Science* **2006,** *314* (5802), 1107.

116. Huang, T. C.; Yeh, J. M.; Lai, C. Y., 18 - Polymer nanocomposite coatings. In *Advances in Polymer Nanocomposites*, Gao, F., Ed. Woodhead Publishing: 2012; pp 605-638.

117. Pastoriza-Santos, I.; Kinnear, C.; Pérez-Juste, J.; Mulvaney, P.; Liz-Marzán, L. M., Plasmonic polymer nanocomposites. *Nature Reviews Materials* **2018,** *3* (10), 375-391.

118. Gao, H.; Lan, X.; Liu, L.; Xiao, X.; Liu, Y.; Leng, J., Study on performances of colorless and transparent shape memory polyimide film in space thermal cycling, atomic oxygen and ultraviolet irradiation environments. *Smart Materials and Structures* **2017,** *26* (9), 095001.

119. Gao, H.; Li, J.; Zhang, F.; Liu, Y.; Leng, J., The research status and challenges of shape memory polymer-based flexible electronics. *Materials Horizons* **2019**.

120. Tonndorf, R.; Kirsten, M.; Hund, R.-D.; Cherif, C., Designing UV/VIS/NIR-sensitive shape memory filament yarns. *Text. Res. J.* **2014,** *85* (12), 1305-1316.

121. Zhang, H.; Xia, H.; Zhao, Y., Optically triggered and spatially controllable shape-memory polymer–gold nanoparticle composite materials. *J. Mater. Chem.* **2012,** *22* (3), 845-849.

122. Mahmoodi, M. J.; Hassanzadeh-Aghdam, M. K.; Ansari, R., Effects of added SiO2 nanoparticles on the thermal expansion behavior of shape memory polymer nanocomposites. *Journal of Intelligent Material Systems and Structures* **2018,** *30* (1), 32-44.

123. Brust, M., Nanoparticle assemblies and superstructures. Edited by nicholas a. Kotov. *Angewandte Chemie International Edition* **2006,** *45* (27), 4399-4399.

124. Gong, J.; Newman, R. S.; Engel, M.; Zhao, M.; Bian, F.; Glotzer, S. C.; Tang, Z., Shape-dependent ordering of gold nanocrystals into large-scale superlattices. *Nature Communications* **2017,** *8*, 14038.

125. Kabb, C. P.; Carmean, R. N.; Sumerlin, B. S., Probing the surface-localized hyperthermia of gold nanoparticles in a microwave field using polymeric thermometers. *Chemical Science* **2015,** *6* (10), 5662-5669.

126. Rahme, K.; Chen, L.; Hobbs, R. G.; Morris, M. A.; O'Driscoll, C.; Holmes, J. D., PEGylated gold nanoparticles: polymer quantification as a function of PEG lengths and nanoparticle dimensions. *RSC Advances* **2013,** *3* (17), 6085-6094.

127. Fratoddi, I., Hydrophobic and Hydrophilic Au and Ag Nanoparticles. Breakthroughs and Perspectives. *Nanomaterials* **2018,** *8* (1).

128. Fernandes, N. J.; Koerner, H.; Giannelis, E. P.; Vaia, R. A., Hairy nanoparticle assemblies as one-component functional polymer nanocomposites: opportunities and challenges. *MRS Communications* **2013,** *3* (1), 13-29.

129. Gabardo, C. M.; Yang, J.; Smith, N. J.; Adams-McGavin, R. C.; Soleymani, L., Programmable wrinkling of self-assembled nanoparticle films on shape memory polymers. *ACS Nano* **2016,** *10* (9), 8829-8836.

130. Toncheva, A.; Khelifa, F.; Paint, Y.; Voué, M.; Lambert, P.; Dubois, P.; Raquez, J.-M., Fast IR-actuated shape-memory polymers using in situ silver nanoparticle-grafted cellulose nanocrystals. *ACS Appl. Mater. Interfaces* **2018,** *10* (35), 29933-29942.

131. Mishra, S. R.; Tracy, J. B., Sequential actuation of shape-memory polymers through wavelength-selective photothermal heating of gold nanospheres and nanorods. *ACS Applied Nano Materials* **2018,** *1* (7), 3063-3067.

132. Bockstaller, M. R.; Lapetnikov, Y.; Margel, S.; Thomas, E. L., Size-Selective Organization of Enthalpic Compatibilized Nanocrystals in Ternary Block Copolymer/Particle Mixtures. *J. Am. Chem. Soc.* **2003,** *125* (18), 5276-5277.

133. Böker, A.; Lin, Y.; Chiapperini, K.; Horowitz, R.; Thompson, M.; Carreon, V.; Xu, T.; Abetz, C.; Skaff, H.; Dinsmore, A. D.; Emrick, T.; Russell, T. P., Hierarchical Nanoparticle Assemblies Formed by Decorating Breath Figures. *Nat. Mater.* **2004,** *3*, 302-306.

134. Bockstaller, M. R.; Mickiewicz, R. A.; Thomas, E. L., Block Copolymer Nanocomposites: Perspectives for Tailored Functional Materials. *Adv. Mater.* **2005,** *17* (11), 1331-1349.

135. Balazs, A. C.; Emrick, T.; Russell, T. P., Nanoparticle Polymer Composites: Where Two Small Worlds Meet. *Science* **2006,** *314* (5802), 1107-1110.

136. Winey, K. I.; Vaia, R. A., Polymer Nanocomposites. *MRS Bull.* **2007,** *32* (4), 314-322.

137. Vaia, R. A.; Maguire, J. F., Polymer Nanocomposites with Prescribed Morphology: Going beyond Nanoparticle-Filled Polymers. *Chem. Mater.* **2007,** *19* (11), 2736-2751.

138. Choi, J. H.; Adams, S. M.; Ragan, R., Design of a Versatile Chemical Assembly Method for Patterning Colloidal Nanoparticles. *Nanotechnology* **2009,** *20* (6), 065301.

139. Zheng, X.; Fontana, J.; Pevnyi, M.; Ignatenko, M.; Wang, S.; Vaia, R.; Palffy-Muhoray, P., The Effects of Nanoparticle Shape and Orientation on the Low Frequency Dielectric Properties of Nanocomposites. *J. Mater. Sci.* **2012,** *47* (12), 4914-4920.

140. Jang, S. G.; Audus, D. J.; Klinger, D.; Krogstad, D. V.; Kim, B. J.; Cameron, A.; Kim, S.-W.; Delaney, K. T.; Hur, S.-M.; Killops, K. L.; Fredrickson, G. H.; Kramer, E. J.; Hawker, C. J., Striped, Ellipsoidal Particles by Controlled Assembly of Diblock Copolymers. *J. Am. Chem. Soc.* **2013,** *135* (17), 6649-6657.

141. Kao, J.; Xu, T., Nanoparticle Assemblies in Supramolecular Nanocomposite Thin Films: Concentration Dependence. *J. Am. Chem. Soc.* **2015,** *137* (19), 6356-6365.

142. Liz-Marzán, L. M., Tailoring Surface Plasmons through the Morphology and Assembly of Metal Nanoparticles. *Langmuir* **2006,** *22* (1), 32-41.

143. Li, Q.; He, J.; Glogowski, E.; Li, X.; Wang, J.; Emrick, T.; Russell, T. P., Responsive Assemblies: Gold Nanoparticles with Mixed Ligands in Microphase Separated Block Copolymers. *Adv. Mater.* **2008,** *20* (8), 1462-1466.

144. Sannomiya, T.; Hafner, C.; Vörös, J., Strain Mapping with Optically Coupled Plasmonic Particles Embedded in a Flexible Substrate. *Opt. Lett.* **2009,** *34* (13), 2009-2011.

145. Kan, T.; Matsumoto, K.; Shimoyama, I. In *Optial measurement of strain using scattering from nanoparticle pairs on elastomer*, 2011 16th International Solid-State Sensors, Actuators and Microsystems Conference, 5-9 June 2011; 2011; pp 1903-1906.

146. Nepal, D.; Onses, M. S.; Park, K.; Jespersen, M.; Thode, C. J.; Nealey, P. F.; Vaia, R. A., Control over Position, Orientation, and Spacing of Arrays of Gold Nanorods Using Chemically Nanopatterned Surfaces and Tailored Particle–Particle–Surface Interactions. *ACS Nano* **2012,** *6* (6), 5693-5701.

147. Kim, Y.; Zhu, J.; Yeom, B.; Di Prima, M.; Su, X.; Kim, J.-G.; Yoo, S. J.; Uher, C.; Kotov, N. A., Stretchable Nanoparticle Conductors with Self-Organized Conductive Pathways. *Nature* **2013,** *500*, 59-63.

148. Gupta, M. K.; König, T.; Near, R.; Nepal, D.; Drummy, L. F.; Biswas, S.; Naik, S.; Vaia, R. A.; El-Sayed, M. A.; Tsukruk, V. V., Surface Assembly and Plasmonic Properties in Strongly Coupled Segmented Gold Nanorods. *Small* **2013,** *9* (17), 2979-2990.

149. Ferrier, R. C.; Lee, H.-S.; Hore, M. J. A.; Caporizzo, M.; Eckmann, D. M.; Composto, R. J., Gold Nanorod Linking to Control Plasmonic Properties in Solution and Polymer Nanocomposites. *Langmuir* **2014,** *30* (7), 1906-1914.

150. Hanske, C.; Tebbe, M.; Kuttner, C.; Bieber, V.; Tsukruk, V. V.; Chanana, M.; König, T. A. F.; Fery, A., Strongly Coupled Plasmonic Modes on Macroscopic Areas via Template-Assisted Colloidal Self-Assembly. *Nano Lett.* **2014,** *14* (12), 6863-6871.

151. Han, X.; Liu, Y.; Yin, Y., Colorimetric Stress Memory Sensor Based on Disassembly of Gold Nanoparticle Chains. *Nano Lett.* **2014,** *14* (5), 2466-2470.

152. Kim, Y.; Yeom, B.; Arteaga, O.; Jo Yoo, S.; Lee, S.-G.; Kim, J.-G.; Kotov, N. A., Reconfigurable Chiroptical Nanocomposites with Chirality Transfer from the Macro- to the Nanoscale. *Nat. Mater.* **2016,** *15*, 461-468.

153. Maldonado, M.; Baltar, H. T. M. C. M.; Gomes, A. S. L.; Vaia, R.; Park, K.; Che, J.; Hsiao, M.; Araújo, C. B. d.; Baev, A.; Prasad, P. N., Coupled-Plasmon Induced Optical

Nonlinearities in Anisotropic Arrays of Gold Nanorod Clusters Supported in a Polymeric Film. *J. Appl. Phys.* **2017,** *121* (14), 143103.

154. Caseri, W., Nanocomposites of Polymers and Metals or Semiconductors: Historical Background and Optical Properties. *Macromol. Rapid Commun.* **2000,** *21* (11), 705-722.

155. Zhang, Y.; Liu, Q.; Mundoor, H.; Yuan, Y.; Smalyukh, I. I., Metal Nanoparticle Dispersion, Alignment, and Assembly in Nematic Liquid Crystals for Applications in Switchable Plasmonic Color Filters and E-Polarizers. *ACS Nano* **2015,** *9* (3), 3097-3108.

156. Caseri, W. R., Dichroic Nanocomposites Based on Polymers and Metallic Particles: From Biology to Materials Science. *Polym. Int.* **2018,** *67* (1), 46-54.

157. Homaeigohar, S.; Elbahri, M., Switchable Plasmonic Nanocomposites. *Adv. Opt. Mater.* **2019,** *7*, 1801101.

158. Zhao, Q.; Qi, H. J.; Xie, T., Recent Progress in Shape Memory Polymer: New Behavior, Enabling Materials, and Mechanistic Understanding. *Prog. Polym. Sci.* **2015,** *49-50*, 79-120.

159. Jain, P. K.; Huang, W.; El-Sayed, M. A., On the Universal Scaling Behavior of the Distance Decay of Plasmon Coupling in Metal Nanoparticle Pairs: A Plasmon Ruler Equation. *Nano Lett.* **2007,** *7* (7), 2080-2088.

160. Sönnichsen, C.; Reinhard, B. M.; Liphardt, J.; Alivisatos, A. P., A Molecular Ruler Based on Plasmon Coupling of Single Gold and Silver Nanoparticles. *Nat. Biotechnol.* **2005,** *23*, 741-745.

161. Qian, Z.; Ginger, D. S., Reversibly Reconfigurable Colloidal Plasmonic Nanomaterials. *J. Am. Chem. Soc.* **2017,** *139* (15), 5266-5276.

162. Murphy, C. J.; Orendorff, C. J., Alignment of Gold Nanorods in Polymer Composites and on Polymer Surfaces. *Adv. Mater.* **2005,** *17* (18), 2173-2177.

163. Pérez-Juste, J.; Rodríguez-González, B.; Mulvaney, P.; Liz-Marzán, L. M., Optical Control and Patterning of Gold-Nanorod–Poly(Vinyl Alcohol) Nanocomposite Films. *Adv. Funct. Mater.* **2005,** *15* (7), 1065-1071.

164. van der Zande, B. M. I.; Pagès, L.; Hikmet, R. A. M.; van Blaaderen, A., Optical Properties of Aligned Rod-Shaped Gold Particles Dispersed in Poly(Vinyl Alcohol) Films. *J. Phys. Chem. B* **1999,** *103* (28), 5761-5767.

165. Li, J.; Liu, S.; Liu, Y.; Zhou, F.; Li, Z.-Y., Anisotropic and Enhanced Absorptive Nonlinearities in a Macroscopic Film Induced by Aligned Gold Nanorods. *Appl. Phys. Lett.* **2010,** *96* (26), 263103.

166. Roskov, K. E.; Kozek, K. A.; Wu, W.-C.; Chhetri, R. K.; Oldenburg, A. L.; Spontak, R. J.; Tracy, J. B., Long-Range Alignment of Gold Nanorods in Electrospun Polymer Nano/Microfibers. *Langmuir* **2011,** *27* (23), 13965-13969.

167. Zhang, H.; Zhang, J.; Tong, X.; Ma, D.; Zhao, Y., Light Polarization-Controlled Shape-Memory Polymer/Gold Nanorod Composite. *Macromol. Rapid Commun.* **2013,** *34* (19), 1575-1579.

168. Fornasiero, D.; Grieser, F., A Linear Dichroism Study of Colloidal Silver in Stretched Polymer Films. *Chem. Phys. Lett.* **1987,** *139* (1), 103-108.

169. Pucci, A.; Bernabò, M.; Elvati, P.; Meza, L. I.; Galembeck, F.; de Paula Leite, C. A.; Tirelli, N.; Ruggeri, G., Photoinduced Formation of Gold Nanoparticles into Vinyl Alcohol Based Polymers. *J. Mater. Chem.* **2006,** *16* (11), 1058-1066.

170. Dirix, Y.; Bastiaansen, C.; Caseri, W.; Smith, P., Oriented Pearl-Necklace Arrays of Metallic Nanoparticles in Polymers: A New Route Toward Polarization-Dependent Color Filters. *Adv. Mater.* **1999,** *11* (3), 223-227.

171. Uhlenhaut, D. I.; Smith, P.; Caseri, W., Color Switching in Gold—Polysiloxane Elastomeric Nanocomposites. *Adv. Mater.* **2006,** *18* (13), 1653-1656.

172. Hribar, K. C.; Metter, R. B.; Ifkovits, J. L.; Troxler, T.; Burdick, J. A., Light-Induced Temperature Transitions in Biodegradable Polymer and Nanorod Composites. *Small* **2009,** *5* (16), 1830-1834.

173. Xiao, Z.; Wu, Q.; Luo, S.; Zhang, C.; Baur, J.; Justice, R.; Liu, T., Shape Matters: A Gold Nanoparticle Enabled Shape Memory Polymer Triggered by Laser Irradiation. *Part. Part. Syst. Charact.* **2013,** *30* (4), 338-345.

174. Zhang, H.; Zhao, Y., Polymers with Dual Light-Triggered Functions of Shape Memory and Healing Using Gold Nanoparticles. *ACS Appl. Mater. Interfaces* **2013,** *5* (24), 13069-13075.

175. Leonardi, A. B.; Puig, J.; Antonacci, J.; Arenas, G. F.; Zucchi, I. A.; Hoppe, C. E.; Reven, L.; Zhu, L.; Toader, V.; Williams, R. J. J., Remote Activation by Green-Light Irradiation of Shape Memory Epoxies Containing Gold Nanoparticles. *Eur. Polym. J.* **2015,** *71*, 451-460.

176. Yao, Y.; Hoang, P. T.; Liu, T., Laser Stimulated Shape Memory Polymer with Inclusion of Gold Nanorod—Effect of Aspect Ratio and Critical Role of On-resonance Irradiation. *J. Mater. Res. Technol.* **2017,** *33* (8), 869-873.

177. Lu, X.; Zhang, H.; Fei, G.; Yu, B.; Tong, X.; Xia, H.; Zhao, Y., Liquid-Crystalline Dynamic Networks Doped with Gold Nanorods Showing Enhanced Photocontrol of Actuation. *Adv. Mater.* **2018,** *30* (14), 1706597.

178. Jie, Y.; Niskala, J. R.; Johnston-Peck, A. C.; Krommenhoek, P. J.; Tracy, J. B.; Fan, H.; You, W., Laterally patterned magnetic nanoparticles. *J. Mater. Chem.* **2012,** *22* (5), 1962-1968.

179. Takahashi, T.; Hayashi, N.; Hayashi, S., Structure and Properties of Shape-Memory Polyurethane Block Copolymers. *J. Appl. Polym. Sci.* **1996,** *60* (7), 1061-1069.

180. Koerner, H.; Kelley, J. J.; Vaia, R. A., Transient Microstructure of Low Hard Segment Thermoplastic Polyurethane under Uniaxial Deformation. *Macromolecules* **2008,** *41* (13), 4709-4716.

181. Mackay, M. E.; Tuteja, A.; Duxbury, P. M.; Hawker, C. J.; Van Horn, B.; Guan, Z.; Chen, G.; Krishnan, R. S., General Strategies for Nanoparticle Dispersion. *Science* **2006,** *311* (5768), 1740-1743.

182. Mangal, R.; Srivastava, S.; Archer, L. A., Phase Stability and Dynamics of Entangled Polymer–Nanoparticle Composites. *Nat. Commun.* **2015,** *6*, 7198.

183. Khlebtsov, N. G., Optics and Biophotonics of Nanoparticles with a Plasmon Resonance. *Quantum Electron.* **2008,** *38* (6), 504-529.

184. Bohren, C. F.; Huffman, D. R., *Absorption and Scattering of Light by Small Particles*. Wiley: New York, N.Y., 1983.

185. Mishchenko, M. I.; Hovenier, J. W.; Travis, L. D., *Light Scattering by Nonspherical Particles: Theory, Measurements and Applications*. Academic: San Diego; London, 2000.

186. Mackowski, D. W.; Mishchenko, M. I., Calculation of the *T* Matrix and the Scattering Matrix for Ensembles of Spheres. *J. Opt. Soc. Am. A* **1996,** *13* (11), 2266-2278.

187. Hovenier, J. W.; Lumme, K.; Mishchenko, M. I.; Voshchinnikov, N. V.; Mackowski, D. W.; Rahola, J., Computations of Scattering Matrices of Four Types of Non-Spherical Particles using Diverse Methods. *J. Quant. Spectrosc. Radiat. Transf.* **1996,** *55* (6), 695-705.

188. Small IV, W.; Wilson, T. S.; Benett, W. J.; Loge, J. M.; Maitland, D. J., Laser-Activated Shape Memory Polymer Intravascular Thrombectomy Device. *Opt. Express* **2005,** *13* (20), 8204-8213.